PEOPLE'S DEMOCRATIC REPUBLIC OF ALGERIA
MINISTRY OF HIGHER EDUCATION AND SCIENTIFIC RESEARCH
University Amar Telidji- Laghouat

Domain: Sciences and Technology

Field: Electrical Engineering

Option: Electrical Power System

Faculty: Technology

Department: Electrical Engineering

Master's dissertation

Presented by: Louassef Mohamed Abd el Rahman

Belkhiri Mohamed Nadhir

Theme

Integration Impact of Electric Vehicles in Low-Inertia Power Networks

Publicly supported ahead of a jury composed of:

Full name	Grade	Quality
Mme. CHETTIH Saliha	Prof	President
*Mr.*OUBBATI Youcef	M.C.A	Examiner
Mr. ARIF Salem	Prof	Supervisor
Mr. ABBOU Aymen	PhD Student	Co-Supervisor

Academic Year 2023-2024

ملخص :يؤدي دمج مصادر الطاقة المتجددة (RESs) في الشبكة الصغيرة إلى انخفاض كبير في القصور الذاتي العام، مما يزيد من قابلية عدم الاستقرار. تؤدي التقلبات في الطلب على الحمل ومخرجات مصادر الطاقة المتجددة إلى تفاقم عدم استقرار التردد. بالإضافة إلى ذلك، عقبة التكلفة المرتفعة للحلول المقترحة السابقة والتي تتمثل في البطاريات (ESS).مما يشكل المزيد من التحديات لإدارة الشبكة. تقترح هذه الأطروحة حل تحكم مبتكر لدمج المركبات الكهربائية (EVs) في شبكات صغيرة منخفضة القصور الذاتي ذات اختراق عالي مستويات الطاقات المتجددة .الهدف الأساسي لنهج التحكم هو تعزيز الاستقرار من خلال الجمع بين التحكم الافتراضي في الدوار لتوفير القصور الذاتي اللازم مع تقنية المشتق التكاملي التناسبي للتخفيف من الآثار الضارة لتأخير قياس الحلقة المغلقة للطور على استجابة التردد. توضح عمليات المحاكاة الشاملة التي تم إجراؤها داخل بيئة MATLAB/Simulink الدور الحاسم لتكامل السيارة الكهربائية في تعزيز استقرار الشبكة الصغيرة .تظهر النتائج أن نشر التحكم الظاهري في الدوار يحسن بشكل كبير استجابة التردد، في حين أن تضمين وحدة التحكم التي تستعمل تقنية المشتق التكاملي التناسبي يؤدي إلى تخفيضات كبيرة في انحرافات التردد. تُظهر استراتيجية التحكم المقترحة مرونة ملحوظة حتى في ظل التغيرات الشديدة في الأحمال وتقلبات الطاقة المتجددة. إن تحسين معلمات التحكم والتحقق من صحتها يسلط الضوء بشكل أكبر على متانة وكفاءة النهج.

الكلمات المفتاحية: مصادر الطاقة المتجددة، القصور الذاتي المنخفض، السيارة الكهربائية، حلقة المغلقة للطور، التحكم الظاهري في الدوار، الشبكة الصغيرة.

Abstract: The integration of Renewable Energy Sources (RESs) in micro grid leads to a significant reduction in overall inertia, heightening susceptibility to instability. Fluctuations in load demand and RESs output exacerbate frequency instability. Additionally,the obstacle is the high cost of previous proposed solutions, which are batteries (ESS). posing further challenges to grid management. This thesis proposes an innovative control solution for the integration of Electric Vehicles (EVs) in low-inertia Microgrids (MGs) with high penetration levels of Renewable Energies (REs). The primary goal of the control approach is to enhance stability by combining Virtual Rotor Control (VRC) to provide the necessary inertia with Proportional Integral Derivative (PID) technique to alleviate the adverse effects of Phase-Locked Loop (PLL) measurement delay on the frequency response. Extensive simulations conducted within the MATLAB/Simulink environment demonstrate the critical role of EV integration in enhancing MG stability. The results show that deploying VRC significantly improves the frequency response, while including the PID controller yields substantial reductions in frequency deviations. The proposed control strategy exhibits remarkable resilience even under severe load variations and RE fluctuations. The optimization and validation of the control parameters further highlight the robustness and efficiency of the approach.

Keywords: Renewable Energy Sources, Low inertia, Electric vehicle (EV), Phased locked loop (PLL), Virtual Rotor Control (VRC), Micro-grid (MG).

Résumé: L'intégration de sources d'énergie renouvelables (SER) dans un micro-réseau entraîne une réduction significative de l'inertie globale, augmentant ainsi la susceptibilité à l'instabilité. Les fluctuations de la demande de charge et de la production des RES exacerbent les instabilités de fréquence. De plus, l'obstacle est le coût élevé des solutions proposées précédemment, qui sont les batteries (ESS). posant ainsi des défis supplémentaires à la gestion du réseau. Cette thèse propose une solution de contrôle innovante pour l'intégration des véhicules électriques (VE) dans des micro-réseaux à faible inertie et à forte pénétration. Niveaux d'énergies renouvelables (ER). L'objectif principal de l'approche de contrôle est d'améliorer la stabilité en combinant le contrôle du rotor virtuel pour fournir l'inertie nécessaire avec la technique de dérivée proportionnelle intégrale (PID) pour atténuer les effets néfastes du retard de mesure de la boucle à verrouillage de phase sur la fréquence. Réponse. Des simulations approfondies menées dans l'environnement MATLAB/Simulink démontrent le rôle critique de l'intégration VE dans l'amélioration de la stabilité du micro-réseau. Les résultats montrent que le déploiement du contrôle virtuel du rotor améliore considérablement la réponse en fréquence, tandis que l'inclusion du contrôleur PID entraîne des réductions substantielles des écarts de fréquence. La stratégie de contrôle proposée présente une résilience remarquable même sous de fortes variations de charge et des fluctuations des ER. L'optimisation et la validation des paramètres de contrôle mettent en évidence la robustesse et l'efficacité de l'approche.

Mots clés : Sources d'Energie Renouvelables, Faible inertie, Véhicule Électrique, Boucle à Verrouillage de Phase, Contrôle Virtuel du Rotor, Micro-réseau.

Dedication

In the name of 'Allah', the Most Gracious and Merciful, who has guided and empowered me throughout this journey.

To my beloved parents, whose boundless love, unwavering support, and relentless belief in me have been the cornerstone of my success. You have instilled in me a passion for learning and excellence that I carry with me always.

I extend my deepest gratitude to my supervisor, Professor ARIF Salem, and Mr. ABBOU Hossam Eddine Aymane, for their steadfast guidance, invaluable mentorship, and unwavering encouragement.

To my dear friends and mentors at the University of Laghouat, your friendship, wisdom, and unwavering support have enriched my journey in countless ways.

Lastly, to my loved ones who have stood by me, offering their unwavering love, encouragement, and understanding, I am profoundly grateful for your presence in my life.

Thank you all for your unwavering support, love, and encouragement.

L. Mohamed

Dedication

First and foremost, I thank Allah for everything.

I dedicate this work to my beloved parents, my sisters, my teachers, and specifically Professor Arif Salem and Dr. Abbou Ayman Hossam Eddine, my relatives, my friends, and my classmates for their encouragement, endless support, valuable comments, advice, time, and patience. They have been the cornerstone of my study. They have been with me every step of the way, through good times and bad. Thank you all for the unconditional love, guidance, and support you have always given me.

B. Mohamed

Acknowledgment

All thanks to, our sincere appreciation are given to our supervisors, **Pr. ARIF Salem** and **Mr. ABBOU Hossam Eddine Aymane,** for their amazing guidance, support and wise words of encouragement from the very beginning and throughout the development of the thesis.

In particular, their gentle and compassionate approach of supervision crucially helped to render the thesis journey a pleasant experience. Without them, this research would not have been possible and we thank also the members of the jury for reading and evaluating our thesis.

We would take this excellent opportunity to express our appreciation to all the teachers who taught us and would also like to thank all the people who have contributed significantly to the achievement of this work and its success.

We are truly grateful.

Content

List of Figures

List of Tables

Nomenclature

Symbols

A_{PV}	The measured area of PV array (m^2)
A_s	The swept area of blade (m^2)
A	Linearly decreased
C	Coefficient vector
C_p	The power co-efficient which is a function of tip speed ratio (λ)
$E_{kinetic}$	Kinetic energy
$F_{ij}^{new,P1}$	Objective function value
H	The inertia constant
K_D	Gain of the derivative action
K_{EVi}	The EV gain
K_I	Gain of the integral action
K_P	Gain of the proportional action

K_{VD}	The virtual damping constant.
K_{VI}	Gain of the virtual inertia
K_i	The area bias
P_{12}	The deviation in tie line power
P_{WT}	The mechanical power output
$P_{inertia}$	Inertia power deviation (p.u)
P_v	The valve position change (p.u)
S_{MG}	The rated microgrid power
S_{SGi}	The rated power of the synchronous generator
T_{EVi}	The time constant of the battery
T_{PV}	The gain constant and the time constant (in seconds) of the SPG
T_{VI}	The virtual inertia time constant
T_{WT}	The gain constant and the time constant (in seconds) of the WPG
T_e	The electrical torque
T_g	Steam turbine speed /governor time constant (s)
T_m	The mechanical torque
$X_{ij}^{new,P1}$	The new status of the *ith* zebra based on first phase
${\Delta P_{AG}}^{max}$	The maximum power output of the EV fleets
${\Delta P_{AG}}^{min}$	The minimum power output of the EV fleets
$\Delta P_{imitate}$	The variation in the active power of the converter/inverter
ΔPL	Load variation (p.u)
ΔPe	Electrical power deviation (p.u)
Δf	Frequency deviation (*Hz*)
$\Delta\omega$	The generator's rotor speed output
E(t)	The error between the desired setpoint and the actual output
S	The system rated power (VA)
n_ω	The velocity of the wind
B	Frequency bias coefficient
D	Damping coefficient
H	The inertia constant
J	The moment of the system inertia (kgm^2)
Ps	The probability of choosing one of two strategies

R	Speed governor (Hz/p.u MW)
ΔP_W	The power output from the WPG (in per unit)
ΔP_e	Electrical power deviation (p.u)
ΔP_g	Generation power deviation (p.u)
ΔP_g	Generation power deviation (p.u)
ΔP_m	Mechanical power deviation (p.u)
η	The conversion efficiency (%) of the PV array
ρ	The air density (kg/m³)
φ	The solar irradiance (W/m^2)
ω	The rotor speed (rad/s),

Acronyms and Abbreviations

ACE	Area Control Error
AGC	Automatic Generation Control
ESS	Energy Storage System
EV	Electric Vehicle
GDB	Governor Dead-Band
GRC	Generation Rate Constraint
IAE	Integral of the Absolute Error
ISE	Integral of the Squared Error
ITAE	Integral of Time multiplied by the Absolute Error
ITSE	Integral of Time multiplied by the Squared Error
LFC	Load Frequency Control
MG	Micro Grid
PFC	Primary Frequency Control
PID	Proportional Integral Derivative
PLL	Phased Locked Loop
RESs	Renewable Energy Sources
ROCOF	The Rate Of Change Of Frequency
SOC	State Of Charge
SPG	Solar Power Generation
VRC	Virtual Rotor Control
WPG	Wind Power Generation
ZOA	Zebra Optimization Algorithm

General Introduction

Problematic

The integration of Renewable Energy Sources (RESs) in power systems is essential for achieving sustainable energy goals. However, this integration presents significant challenges due to the inherently low inertia of RESs. Inertia in power systems is crucial for maintaining stability and responding to sudden changes in load and generation. The overall inertia of an interconnected power system can be significantly reduced due to the high penetration of RESs, which lack the physical rotating mass that provides inertia.

This reduction in inertia increases the susceptibility of the power system to instability. Fluctuations in load and RES generation contribute to instabilities in the system's frequency, posing a significant challenge to maintaining grid stability. Furthermore, integrating A phase-locked loop (PLL) is a closed-loop system in which an internal oscillator is controlled to keep the time of some external periodical signal by using the feedback loop, it serves to measure frequency and synchronize with the grid. Given that VRC involves converters, it relies on PLL for swift responses to changes in micro grid (MG) frequency However it introduces time delays, noises, and oscillations to the system

Another challenge is the high cost associated with battery storage systems, which are often proposed as a solution to stabilize the grid amidst renewable energy fluctuations. These expenses impact the feasibility and economic viability of using batteries to manage grid stability.

Therefore, innovative control solutions are required to address these challenges. This thesis proposes an innovative control solution that integrates Electric Vehicles (EVs) into low-inertia Microgrids (MGs) with high levels of RES penetration. The control approach combines Virtual Rotor Control (VRC) to provide the necessary inertia with a Proportional Integral Derivative (PID) technique to mitigate the adverse effects of Phase-Locked Loop (PLL) measurement delays on the frequency response.

Brief Survey of Virtual Rotor control

Over the years, research has explored various control strategies to address the challenge of high-RES penetration and its impact on system inertia. For instance, authors in [1] introduce a Virtual Inertia Control (VIC) method that concurrently addresses damping and inertia properties, significantly enhancing Microgrid stability with high-RES integration. Other studies have embedded Model Predictive Control (MPC) into VIC for a more robust response in low-inertia Microgrids [2,3]. Additionally, the work presented in [4] proposes an optimized fractional-order integral (iFOI) controller, utilizing the Gray Wolf Optimization (GWO) algorithm, to improve load frequency control (LFC) in modern power systems facing low inertia. Another research employs a variable fractional-order PID controller for virtual inertia control, utilizing online tuning through a modified neural network-based algorithm trained with deep reinforcement learning [5]. A study in [6] proposes a rule-based self-adaptive Virtual Inertia Control (VIC) technique based on fuzzy logic control principles to address the challenge of maintaining frequency stability. Another work introduces a robust control strategy employing a coefficient diagram method (CDM) for load frequency control (LFC) in Smart Hybrid Power Systems (SHPSs), considering factors like high-RES penetration and Electric Vehicle (EV) integration, to ensure stability against various perturbations, system uncertainties, and physical constraints [7]. Additionally, some research has explored the application of Superconducting Magnetic Energy Storage (SMES) in lieu of ESS within Virtual Inertia Control (VIC) frameworks, as seen in [8].

Furthermore, Fractional Order PID (FOPID) controllers provide several benefits, including improved robustness, wider stability margins, and greater flexibility in shaping frequency responses compared to integer order counterparts. They demonstrate exceptional performance in systems with non-integer order dynamics. Furthermore, FOPID controllers exhibit superior transient response, adapt effectively to time-varying systems, and are less affected by inaccuracies in the model. In summary, they stand as a potent instrument for attaining precise and resilient control in diverse dynamic systems [9].

Beyond these technological advancements, plug-in EVs have become dynamic assets within the power system. They actively participate in grid operations by acting as flexible energy storage resources. With appropriate control strategies, EVs can intelligently adjust their charging and discharging rates based on the Microgrid needs, allowing for better integration of

RES and enhanced stability. For instance, during peaks of RES production, excess energy can be stored in EV batteries, acting as a buffer. Conversely, during valleys, EVs can discharge power back into the grid to help stabilize the frequency [10].

Objectives of This Thesis

The main objectives of this thesis, derived from the identified problems, are as follows:

- To investigate the impact of significantly reduced overall inertia in interconnected power systems due to the high penetration of RESs and develop strategies to mitigate the associated instability.
- To implement a technique to mitigate the adverse effects of Phase-Locked Loop (PLL) measurement delays on the frequency response.
- To reduce the cost of classic batteries by replacing them with EVs which is a better cost friendly alternative.

Thesis Outlines

This Thesis is divided into three main chapters as follows:

Chapter One: Automatic generation control with RES

This chapter describes AGC control loops and some models are given. Then, the Proportional-Integral-Derivative (PID) Regulator and a number of non-linear constraints are presented and discussed. Also, a description about the detailed linearized models of Wind Power Generation (WPG) unit and Solar Power Generation (SPG) unit is given. Finally, exploring low inertia and its effects.

Chapter Two: Virtual rotor control-based EV

This chapter addresses several crucial aspects in the field of AGC. Then, it delves into Virtual Rotor Control technique based on derivative methodology to emulate both inertia and provide damping synchronously. It discusses frequency regulation concerning inertia control and the impact of the Phase-Locked Loop (PLL) control loop. Additionally, it sheds light on the role of electric vehicles in improving grid performance by providing virtual inertia. The chapter concludes by a proposed model and using a new optimization algorithm called the "Zebra Optimization Algorithm" (ZOA).

Chapter Three: Simulation and results

This chapter addresses several fundamental aspects, starting with the description of the investigated micro grid using the proposed controllers and studying the impact of the Phase-Locked Loop (PLL) on the microgrid. Additionally, the chapter provides optimal control settings for Proportional-Integral-Derivative (PID) controllers and Virtual Rotor Control (VRC) enhanced with the Zebra Optimization Algorithm (ZOA). Furthermore, it analyzes the impact of the measurement delay on the performance of VRC. It also tests the effectiveness of implementing the proposed control technic for electric Vehicles under step load changes. Finally, it highlights the robustness of the proposed control technique by subjecting the system to random fluctuations in renewable energy sources and load.

Chapter I: Automatic Generation Control with RESs

I.1. Introduction

Automatic generation control (AGC) is one of the important control problems in electric power system design and operation, it is becoming more important nowadays as renewable energy sources (RESs) such as wind and solar farms proliferate. The power fluctuation induced by a large penetration of wind and solar farms contributes to power imbalance and frequency variation in a negative way [10]. In this chapter, we're going to talk about the various AGC control loops and some models are given. Then, the Proportional-Integral-Derivative (PID) Regulator and a number of non-linear constraints are presented and discussed. Also, a description about the detailed linearized models of Wind Power Generation (WPG) unit and Solar Power Generation (SPG) unit is given. Finally, exploring low inertia and its effects.

I.2 Active Power and Frequency Control

A power system is crucial for efficiently transmitting power, aiming for uninterrupted supply. However, maintaining normal conditions constantly is challenging. Typically, machines operate normally over 99% of the time, with bus voltage and frequency regulated to balance active and reactive control. System "normality" relies on the equilibrium between generation and demand.

A constant frequency is indicative of a smoothly operating system. This stability is essential for various reasons: AC motors' speeds are directly tied to frequency, generator turbines, especially steam turbines, operate optimally at specific speeds, and managing total power device output is more efficient within strict frequency limits [10].

I.2.1. Load Frequency Mechanism

The load frequency mechanism ensures that the frequency of the power system remains stable, reflecting the balance between generation and consumption. In normal operation, generators produce power slightly higher than what's needed to account for transmission losses. Since electrical energy storage is challenging, generation must match consumption rates.

As the system load fluctuates, generation must adapt to maintain a balance and minimize power imbalances. This adjustment is achieved through primary and secondary control loops, which work to restore any deviations between actual frequency (Af) and planned frequency (AP) to zero, counteracting disturbances in the system.

I.2.2. Primary and Secondary Controls Action

Primary and secondary control actions play vital roles in maintaining the system frequency within acceptable limits. The frequency of the power system is directly influenced by the balance between load and generation. Any disparity between load and generation results in frequency deviations.

Control mechanisms for managing generated power and frequency in extensive power systems are often termed load-frequency control (LFC). These controls ensure that any discrepancies between load and generation are swiftly corrected to prevent frequency deviations, thus ensuring the stability and reliability of the power system [11].

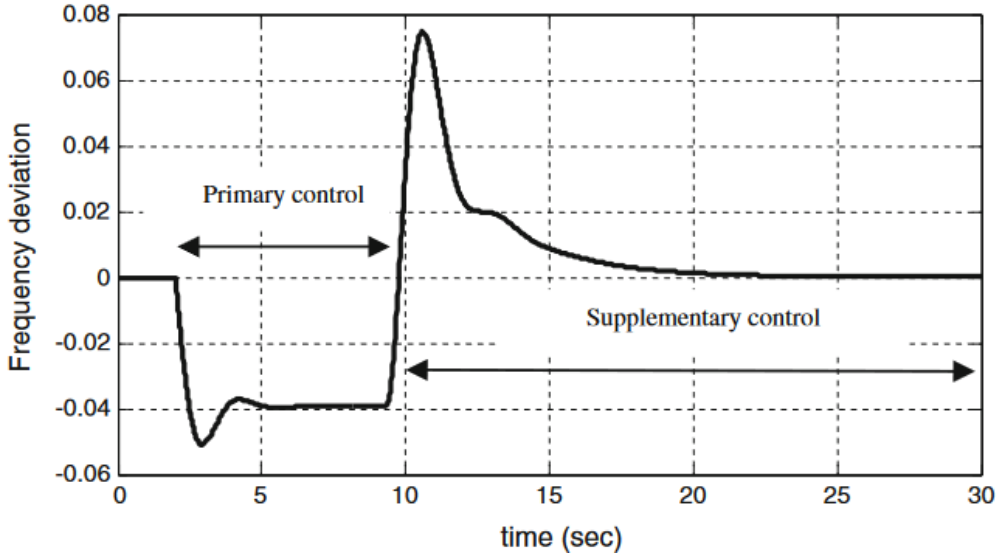

Fig. I.1: Frequency deviation responses (Hz) in primary and supplementary controls [2]

I.2.3. Primary Control

Primary control is crucial for regulating the real power output of generators, which is determined by the mechanical power output of prime movers like steam turbines, gas turbines, hydro turbines, or diesel engines. The flow of steam or water into the turbine input is adjusted by opening or closing valves to control mechanical power. It's essential to maintain a constant

balance in the input of steam or water to meet the demand for real power. Without this regulation, the machine's speed would fluctuate, leading to frequency changes that could disrupt the satisfactory operation of the power system. Thus, primary control ensures that the frequency remains nearly constant for the power system to function effectively [12].

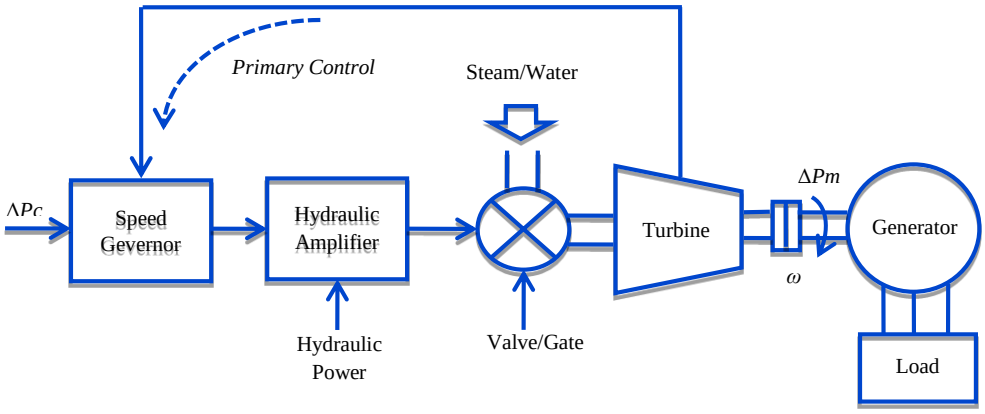

Fig. I.2: Governor-Turbine with primary frequency control loop.

The schematic block diagram in Fig. I.1 illustrates a synchronous generator equipped with a primary frequency control loop. The speed governor within the primary control loop detects speed changes. In practice, primary control initiates local automatic control to provide reserve power against frequency changes. A hydraulic amplifier facilitates mechanical force to adjust the main valve against high steam pressure or hydro, maintaining a steady-state power output for the turbine.

Each generator's speed governor offers primary speed control, contributing to overall generation transition regardless of load shift locations. However, primary control intervention alone may not adequately restore system frequency, especially in an interconnected power system, and the supplementary control loop is required to adjust the load reference setting point through the speed changer motor [12].

I.2.4. Secondary Control

The secondary control loop, alongside primary frequency control, can be implemented in a large synchronous generator. Fig I.3 illustrates a schematic block diagram of a synchronous generator equipped with both primary and secondary frequency control loops.

The secondary loop offers feedback via frequency deviation and incorporates it through a dynamic controller into the primary control loop. The resulting signal (APc) is utilized to regulate the system's frequency. In practical power systems, the dynamic controller is typically a straightforward integral or proportional-integral controller (PI).

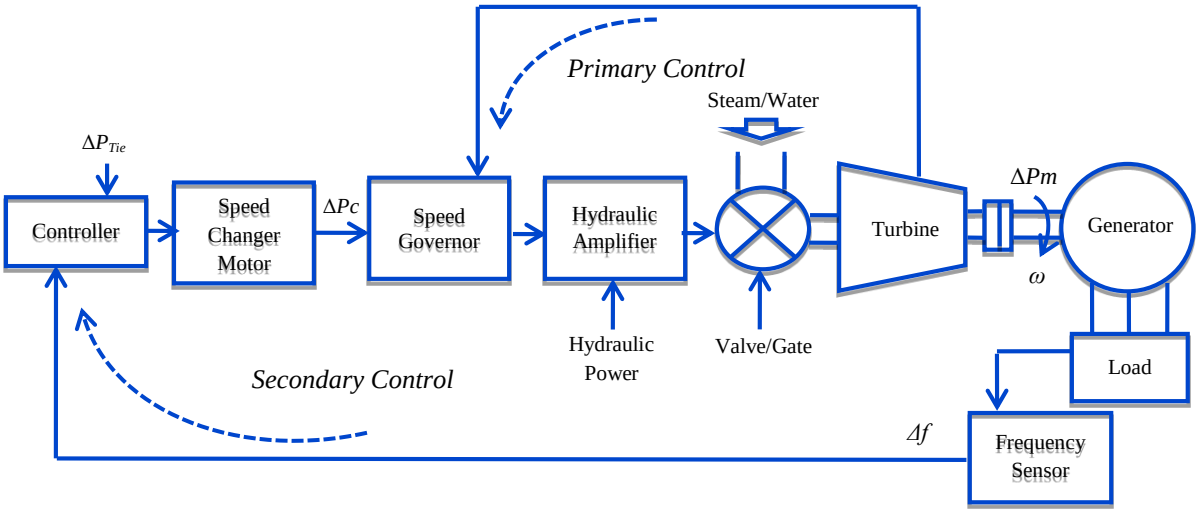

Fig. I.3: Frequency control mechanism of primary and secondary operation

After a load change, the feedback mechanism provides a suitable signal for the turbine to track the load and restore the frequency of the system. Secondary frequency control, also known as load frequency control (LFC), is a critical function of AGC systems as they operate online to manage system frequency and power generation. The effectiveness of AGC depends heavily on how participating generating units respond to control signals.

During a sudden increase in area load, the frequency experiences a temporary drop. Power flows from other areas transiently to supply the excess load. Typically, all generating units within each area adjust to accommodate this load change. In steady state, generators closely match the load, allowing tie-line power and frequency variations to decrease to zero [12].

I.3. Models for Generators and Loads

Power system loads consist of diverse electrical devices. Resistive loads, such as lighting and heating elements, are insensitive to frequency changes, whereas motor loads react to frequency

variations [13]. The aggregate frequency-dependent behavior of a composite load can be approximated by the equation (I.1):

$$\Delta Pe = \Delta P_L - D\,\Delta\omega \tag{I.1}$$

Where a 1% frequency change is commonly represented by a percentage change in load [13].

This section introduces a simplified frequency response model for the depicted schematic block diagram in Fig I.1, featuring a single generator unit. The dynamic relationship between the incremental mismatch power ($\Delta \boldsymbol{P_m}$ - $\Delta \boldsymbol{P_L}$) and the generator's rotor speed output ($\boldsymbol{\Delta\omega}$) (which corresponds to the frequency of the power systems) can be described by [14]:

$$\Delta P_{m(t)} - \Delta P_{e(t)} = 2H\frac{d\Delta\omega(t)}{dt} \tag{I.2}$$

$$\Delta P_{m(t)} - \Delta P_L(t) = 2H\frac{d\Delta\omega(t)}{dt} + D\Delta\omega(t) \tag{I.3}$$

Utilizing the Laplace transform, equation (I.3) can be expressed as:

$$\Delta P_{m(s)} - \Delta P_L(s) = 2H\,s\Delta\omega(s) + D\Delta\omega(s) \tag{I.4}$$

$$\Delta\omega(s) = \left(\frac{1}{2Hs + D}\right) * \left(\Delta P_{m(s)} - \Delta P_L(s)\right) \tag{I.5}$$

Where D is Load change and H is Inertia control ΔP_L is Load power change ΔP_m is Mechanical power change, Δω is generator's rotor speed output.

Equation (I.5) can be depicted in a block diagram as shown in Fig.I.4.

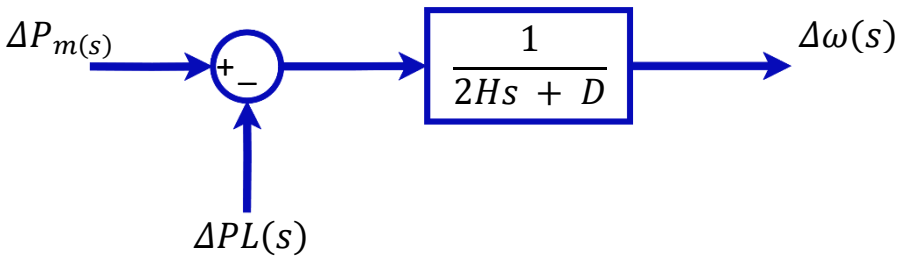

Fig. I.4: Generator and load block diagram

I.4. Models for Turbines and Governors

The prime mover, such as hydraulic turbines for waterfalls, steam turbines fueled by coal, gas, or nuclear energy, or gas turbines, is the primary source of mechanical power. Turbine models relate changes in mechanical power output (ΔPm) to variations in steam valve position (ΔPv). Different turbine types exhibit diverse characteristics [15].

I.4.1. Steam Turbine Model

For non-reheat steam turbines, the simplest prime mover model can be approximated with a single time constant T_T [15]. The transfer function for a non-reheat turbine is defined as:

$$G_{T(s)} = \frac{\Delta P_{m(s)}}{\Delta P_{v(s)}} = \frac{1}{1 + T_T s} \tag{I.6}$$

The block diagram for a simple non-reheat steam turbine is illustrated in Fig I.5.

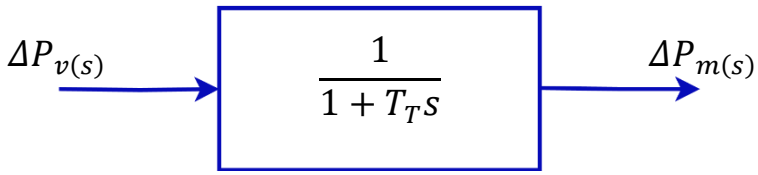

Fig. I.5: Block diagram for a simple non-reheat steam turbine

I.4.2. Governor

The regulation of real power in a power system is achieved by adjusting the driving torques of individual turbines (steam or hydro). By controlling the position, denoted by *XE*, of the governor-controlled valves (or gates for hydro-turbines), flow control over high-pressure steam (or water) through the turbine is achieved. Modern governors typically employ electronic devices to detect speed changes. Fig I.5 schematically displays the essential elements of a standard watt governor [16].

By adjusting the set point, a desired load dispatch can be scheduled at nominal frequency. To ensure stable operation, governors are designed to allow the speed to decrease as the load increases [17].

$$\Delta P_g = \Delta P_{ref} - \left(\frac{1}{R}\right)\Delta\omega \tag{I.7}$$

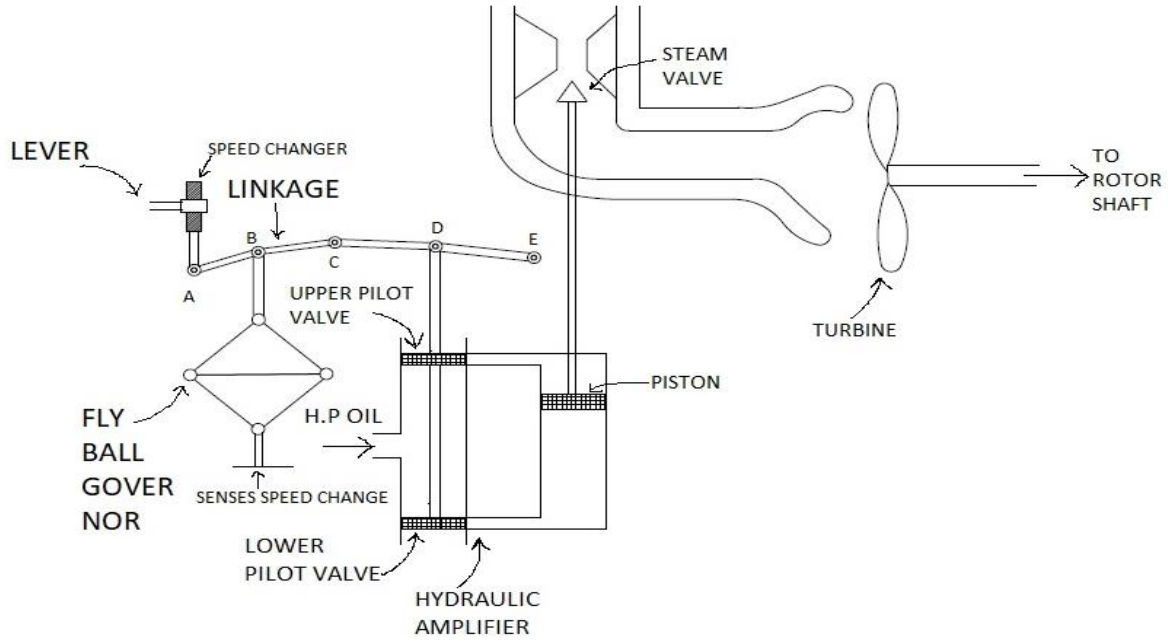

Fig. I.6: Speed governing system.

By adjusting this set point, a desired load dispatch can be scheduled at nominal frequency.

In the Laplace domain:

$$\Delta P_{g(s)} = \Delta P_{ref(s)} - \left(\frac{1}{R}\right)\Delta\omega(s) \tag{I.8}$$

Assuming a linear time constant, the command ΔPg is converted into the steam valve position command ΔPv, yielding the relation in the Laplace domain:

$$\Delta P_{v(s)} = \frac{\Delta P_{g(s)}}{1 + T_g S} \tag{I.9}$$

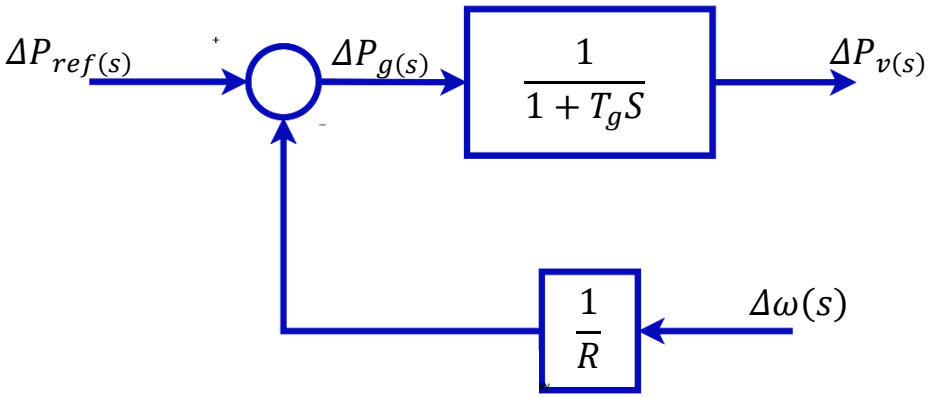

Fig. I.7: Block diagram representation of speed governing system for steam turbine

I.5. Control Models for Power Systems

In understanding power system configurations, predominant focus lies on employing linearized models for both single-area and multi-area power systems. This segment delves into various approaches to frequency control within significant power system frameworks.

I.5.1. Automatic Generation Control (AGC) in Single-Area Systems

In a single-area system, alterations in system load provoke a steady-state frequency deviation, contingent upon governor speed regulation. To nullify this frequency deviation, a corrective measure is essential. This correction can be accomplished by integrating a controller that acts upon the load reference setting, thereby adjusting the speed set point. The integration of such a controller increases the system's type by one, ensuring the final frequency deviation reaches zero. Proper adjustment of the integral controller gain, denoted as *K*, is crucial for achieving an acceptable transient response [15].

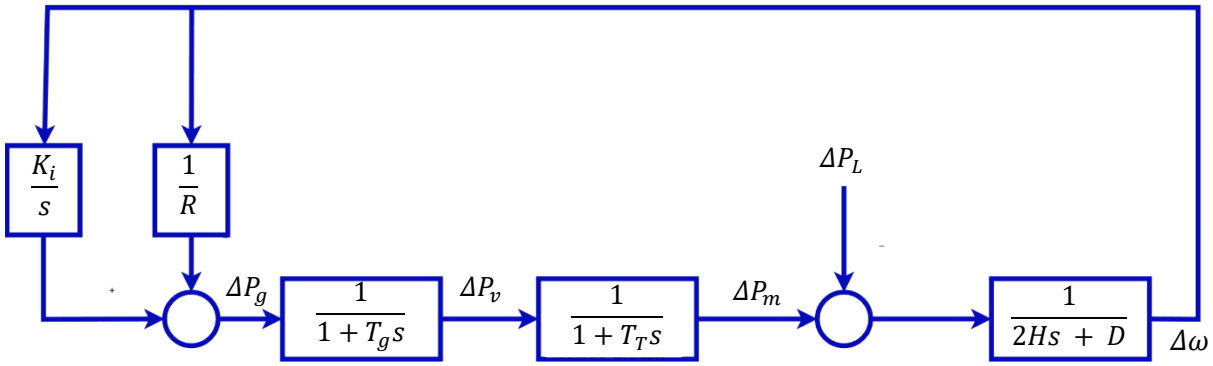

Fig. I.8: AGC for an isolated power system with secondary control.

a) Two-Area System with Primary Control

In a scenario involving two areas interconnected by a lossless tie line with a reactance denoted as X_{tie}, each area is symbolized by an equivalent generating unit linked by a voltage source behind an equivalent reactance, illustrated [18]:

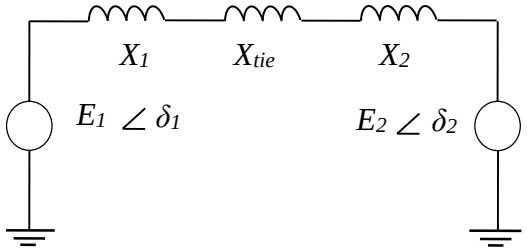

Fig. I.9: Equivalent network for two area power system

During normal operation, the real power transmitted across the tie line is determined by:

$$P_{12} = \frac{|E_1||E_2|}{X_{12}} \sin \delta_{12} \tag{I.10}$$

Where: $X_{12} = X_1 + X_{tie} + X_2$, and $\delta 12 = \delta 1 - \delta 2$.

The deviation in tie line power manifests as (where P_s is the slope of the power curve at the initial operating angle):

$$P_{12} = P_s (\Delta\delta_1 - \Delta\delta_2) \tag{I.11}$$

This tie line power fluctuation simulates an increase in load in one area and a decrease in load in the other, contingent upon the flow direction. The direction of current flow is dictated by the phase angle difference; if $\Delta\delta 1 > \Delta\delta 2$, power moves from area 1 to area 2 [13].

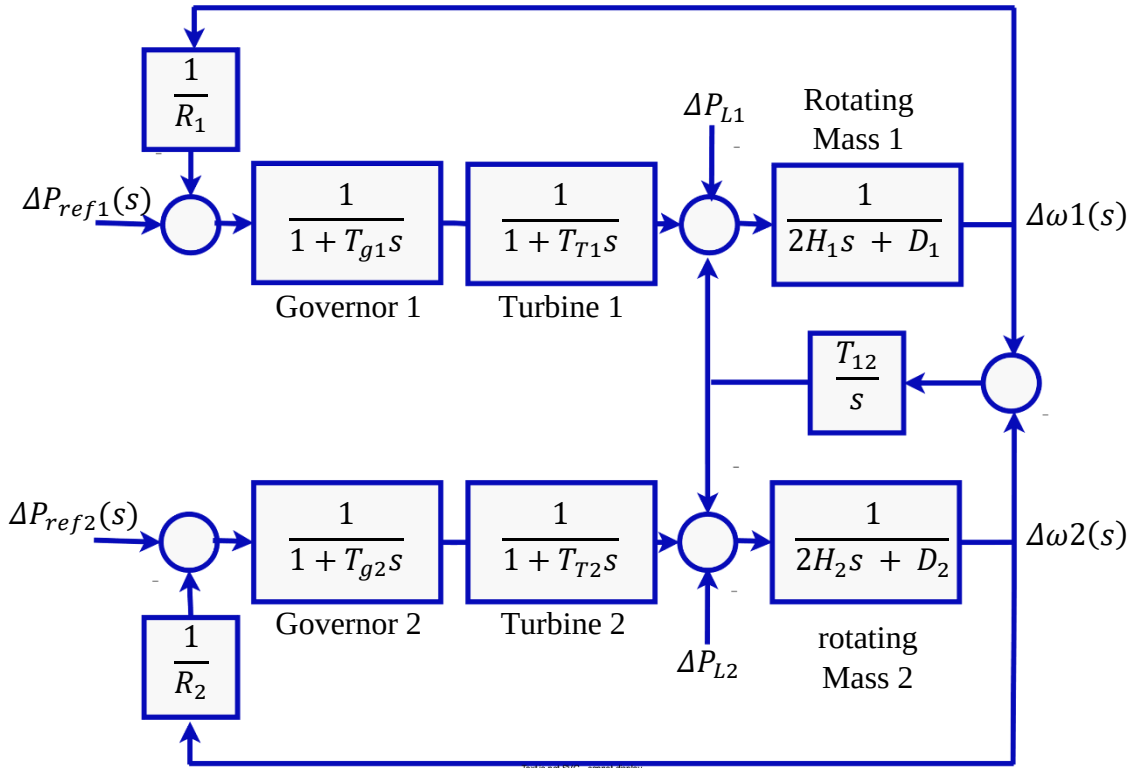

Fig. I.10: Two area system with primary LFC loop

b) Two-Area System with Secondary Control

During normal operation of the power system, ensuring the areas' demands are met at the nominal frequency, a straightforward control strategy is adopted [13]:

- Maintaining the frequency at its nominal value.

- Regulating the tie-line flow as per schedule.

- Each zone independently managing its own loads.

In a two-area system, each area endeavors to minimize its Area Control Error (ACE) to zero, expressed as follows:

$$ACE_i = \sum \Delta P_{ij} + K_i \Delta\omega_j \qquad (n = 1 \; to \; j) \tag{I.12}$$

Where K_i, termed as the area bias, determines the degree of interaction during disturbances in neighboring areas. Optimal performance is achieved when K_i equals the frequency bias factor of the respective area. The ACEs for both areas are delineated as [13]:

$$ACE_1 = \Delta P_{12} + B_1 \Delta\omega_1 \quad \text{(I.13)}$$

$$ACE_2 = \Delta P_{21} + B_2 \Delta\omega_2 \quad \text{(I.14)}$$

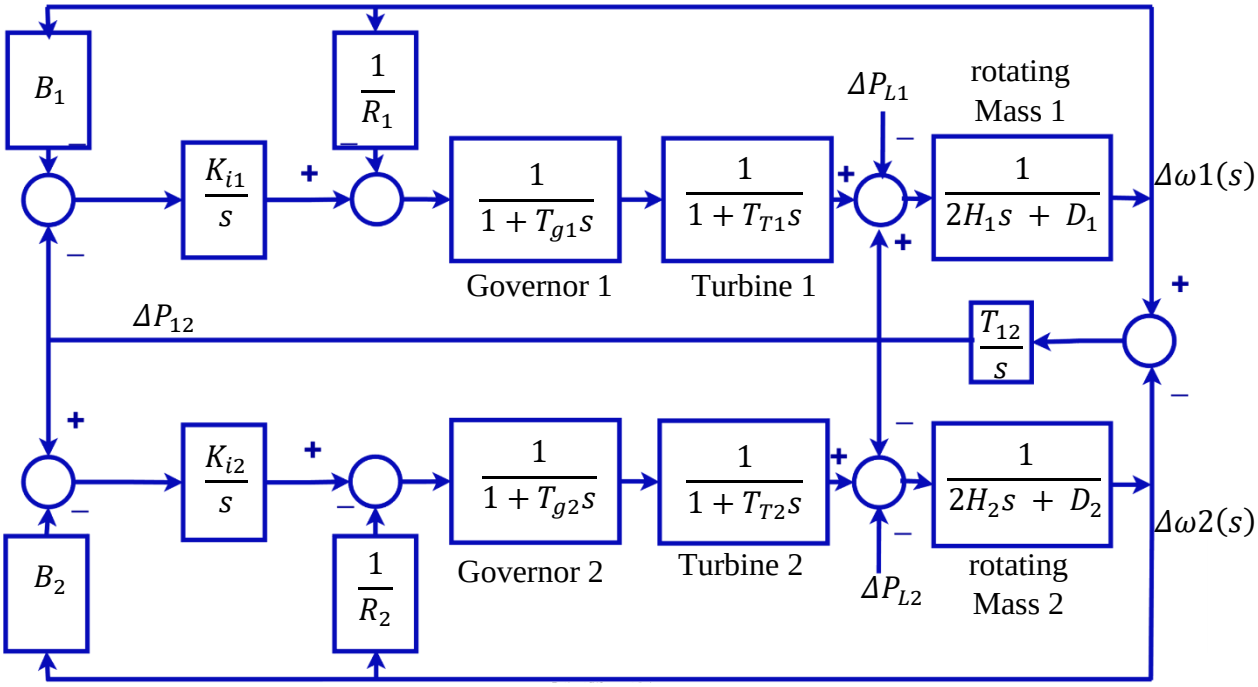

Fig. I.11: Block diagram of a basic AGC for two area system

I.6. Proportional-Integral-Derivative (PID) Regulator

A PID Controller can be conceptualized as an extreme version of a phase lead-lag compensator, with one pole at the origin and the other at infinity. Likewise, its counterparts, the Proportional-Integral (PI) and Derivative (PD) regulators, can be seen as extreme instances of phase-lag and phase-lead compensators, respectively [14]. A typical PID controller, often referred to as the "three-term" controller, is represented by a transfer function commonly expressed in the "parallel form" as:

$$S = K_P + K_I \frac{1}{s} + K_D . s \quad \text{(I.15)}$$

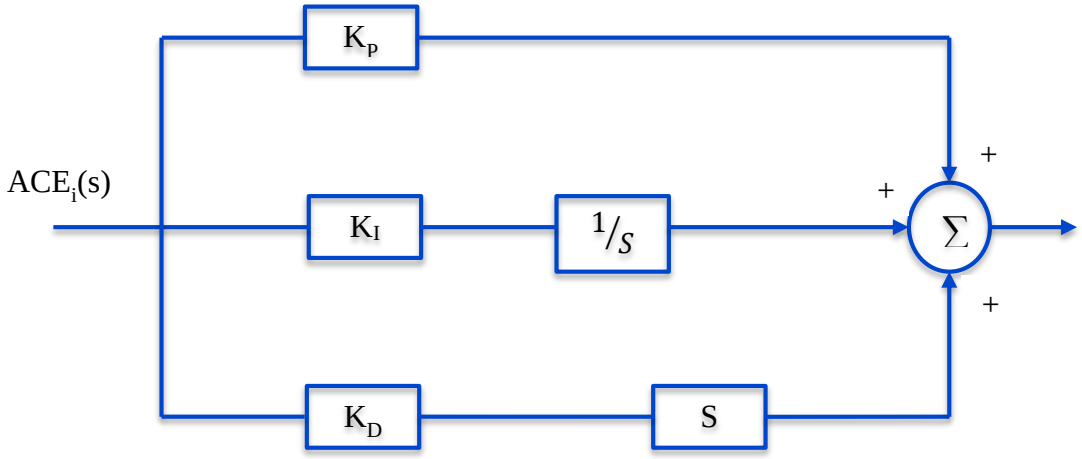

Fig. I.12: PID control scheme "parallel form"

Here, K_P denotes the proportional gain, K_I represents the integral gain, and K_D signifies the derivative gain [14].

- The proportional term K_P: Governing the control behavior in proportion to the error signal through the all-pass gain factor.

- The integral term K_I : Mitigating steady-state errors by providing low-frequency compensation through integration.

- The derivative term K_D : Enhancing transient response by offering high-frequency compensation through differentiation.

I.7. Consideration of Physical Constraints

To enhance the realism of outcomes, it's imperative to incorporate nonlinear constraints such as the Generation Rate Constraint (GRC) and the Speed Governor Dead-Band (GDB).

I.7.1. Generation Rate Constraint

A critical constraint in power system AGC is the Generation Rate Constraint (GRC), which limits the rate of mechanical movement variation. The block diagram depicted in Fig. I.14 illustrates a non-linear turbine model incorporating GRC [20].

The acceptable rate of power output change for generating units engaged in AGC must align with the overall objectives of AGC. This is typically expressed as a percentage of the control

generator's rated output per unit of time. Different types of generation units exhibit varying rates, with typical ramp rates provided as percentages of capacity per minute for various technologies. For instance, diesel engines, industrial gas turbines (GT), combined cycle GT, steam turbine plants, and nuclear power plants have typical ramp rates ranging from 40%/min to 1% to 5%/min, respectively. The rates for hard-coal and lignite-fired power plants are in the range of 2 to 4% per minute and 1 to 2% per minute, respectively.

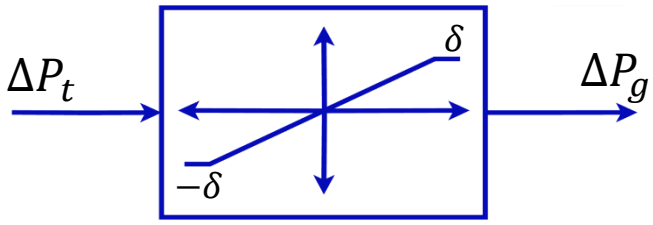

Fig. I.13: Non-linear turbine model with GRC

I.7.2. Speed Governor Dead-Band

Another significant physical constraint is the Speed Governor Dead-Band (GDB), defined as the total magnitude of a sustained speed change within which there's no corresponding valve position change. The specified limit for the dead band is typically set at 0.06% (*0.036Hz*). GDB strongly influences governor performance and can destabilize system transient performance. A wider dead band can notably degrade AGC performance by increasing the apparent steady-state frequency control. The block diagram model illustrating speed governor dead-band is depicted in Fig. I.14 [13].

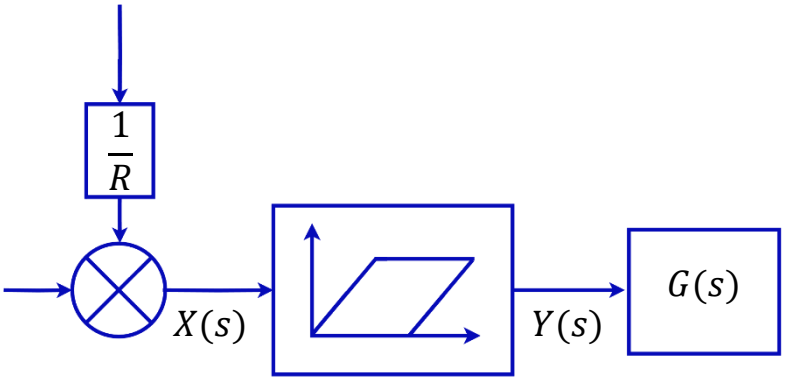

Fig. I.14: Block diagram model of speed governor dead-band

I.8. Integration of AGC with Renewable Energy Options

The structure of power systems is undergoing fundamental transformations, spurred by deregulation, competitive policies, and the adoption of diverse renewable energy sources (RESs). The increasing demand for electrical energy, coupled with finite fossil fuel resources and escalating environmental concerns, underscores the necessity for rapid advancements in RESs. Renewable energy harnessed from natural sources like the sun, wind, hydropower, biomass, geothermal, and oceans is gaining prominence. Consequently, contemporary power systems necessitate novel AGC methodologies.

Research indicates that integrating renewables into the grid affects system frequency and power fluctuation, with effects growing more pronounced as penetration levels increase. Variability and unpredictability are inherent traits of variable RESs such as wind, solar, and wave energy, posing significant challenges to bulk power system planning and operations [13].

I.8.1. Impact of Renewable Energy Sources (RESs) on Power Systems

RESs influence the dynamic behavior of power systems in ways distinct from conventional generators. Unlike conventional plants utilizing synchronous generators capable of sustained operation during significant transient faults, if a substantial portion of wind or solar generation is disrupted due to a fault, the adverse effects on power system control, including frequency regulation issues, could escalate. High penetration of renewable energy in power systems may amplify uncertainties during abnormal operation, posing several technical challenges and raising pertinent questions regarding the adequacy of traditional power system control methodologies in this new landscape.

The integration of RESs into power system grids affects various aspects, including optimum power flow, power quality, voltage and frequency control, system economics, and load dispatch. Given the inherent variability in RESs power output, increasing attention has been directed towards understanding their impact on frequency regulation over the past decade. Substantial interconnection frequency deviations can trigger under/over-frequency relaying, leading to disconnection of loads and generation sources. Under unfavorable conditions, this may culminate in cascading failures and system collapse [22].

I.8.2. AGC Model Incorporating RESs

In this model, Automatic Generation Control (AGC) is applied to a two-area power system integrated with two distinct Renewable Energy Sources (RESs): area-1 with Solar Power Generation (SPG) and area-2 with Wind Power Generation (WPG).

a) Modeling of Wind Power Generation (WPG)

Wind Power Generation (WPG) is garnering increasing interest as a viable alternative energy source, particularly following solar energy. It proves to be a more effective and readily available energy producer in many regions worldwide. Several countries are now opting for WPG as a promising alternative energy solution [23].

In the case of WPG, wind turbines harness the kinetic energy of the wind and convert it into mechanical power output (P_{WT}). This mechanical power output from the wind turbine is then transmitted to the rotor of the generator, where it is converted into electrical power (P_{WTg}) via the turbine-generator shaft.

The governing equations that represent the mechanical power output from the wind turbine can be expressed as follows [23]:

$$P_{WT} = \frac{1}{2}\rho A_s C_p (v\omega)^3 \tag{I.16}$$

Where ρ represents the air density (kg/m³), A_s is the swept area of the blade (m^2), v denotes the wind velocity, and C_p is the power coefficient, dependent on the tip speed ratio (λ) and blade pitch angle (β) [24]. WPG operates as a non-linear system. However, for the purposes of this study, we adopt a simplified linearized model of the WPG, represented by a first-order lag transfer function model G_{WPG} (s), as illustrated below:

$$G_{WPG} = \frac{\Delta P_W}{\Delta P_{Wind}} = \frac{1}{1 + sT_{WT}} \tag{I.17}$$

Where ρ represents the air density (kg/m³), A_s is the swept area of the blade (m^2), v denotes the wind velocity, and C_p is the power coefficient, dependent on the tip speed ratio (λ) and blade pitch angle (β) [24]. WPG operates as a non-linear system. However, for the purposes of this study, we adopt a simplified linearized model of the WPG, represented by a first-order lag transfer function model G_{WPG} (s), as illustrated below.

Fig. I.15: Linearized model of WPG

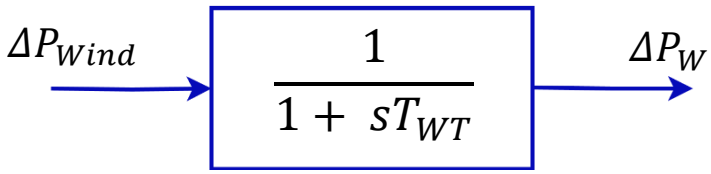

b) Modeling of Solar Power Generation (SPG)

SPG emerges as a promising RES due to its CO2-free power production, flexibility, and simplicity. Despite being dependent on solar irradiance and temperature, SPG offers significant advantages, including minimal maintenance, absence of moving parts, noise-free operation, and environmentally friendly energy conversion. The electrical power output (P_{SPG}) from SPG systems can be expressed by a governing equation, with a simplified linearized model represented as a first-order lag transfer function G_{SPG} (s). The model parameters include the gain constant (T_{PV}) and time constant (in seconds) of the SPG [25].

$$P_{SPG} = \eta\varphi A_{PV}\{1 - 0.005\,(Ta + 25)\} \tag{I.18}$$

Where η is the conversion efficiency (%) of the PV array, φ is the solar irradiance (W/m^2), APV is the measured area of PV array (m^2) and Ta is the ambient temperature (C°). In the present work, linearized mathematical model of the SPG is incorporated and represented as the first-order lag transfer function model G_{SPG} as shown in:

$$G_{SPG} = \frac{\Delta P_S}{\Delta P_{SOLAR}} = \frac{1}{1 + sT_{PV}} \tag{I.19}$$

Where T_{PV} the gain constant and the time constant (s) of the SPG, respectively.

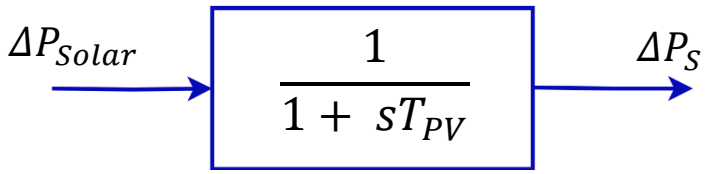

Fig. I.16: Linearized model of SPG

I.9. AGC with RESs Model

In this section, we will present a model of Automatic Generation Control (AGC) for a two-area interconnected thermal power system incorporating Renewable Energy Sources (RESs) such as solar and wind power generation. Each area within the system consists of a speed governing system, turbine, generator, Governor Dead Band (GDB), and Governor Rate Constraint (GRC).

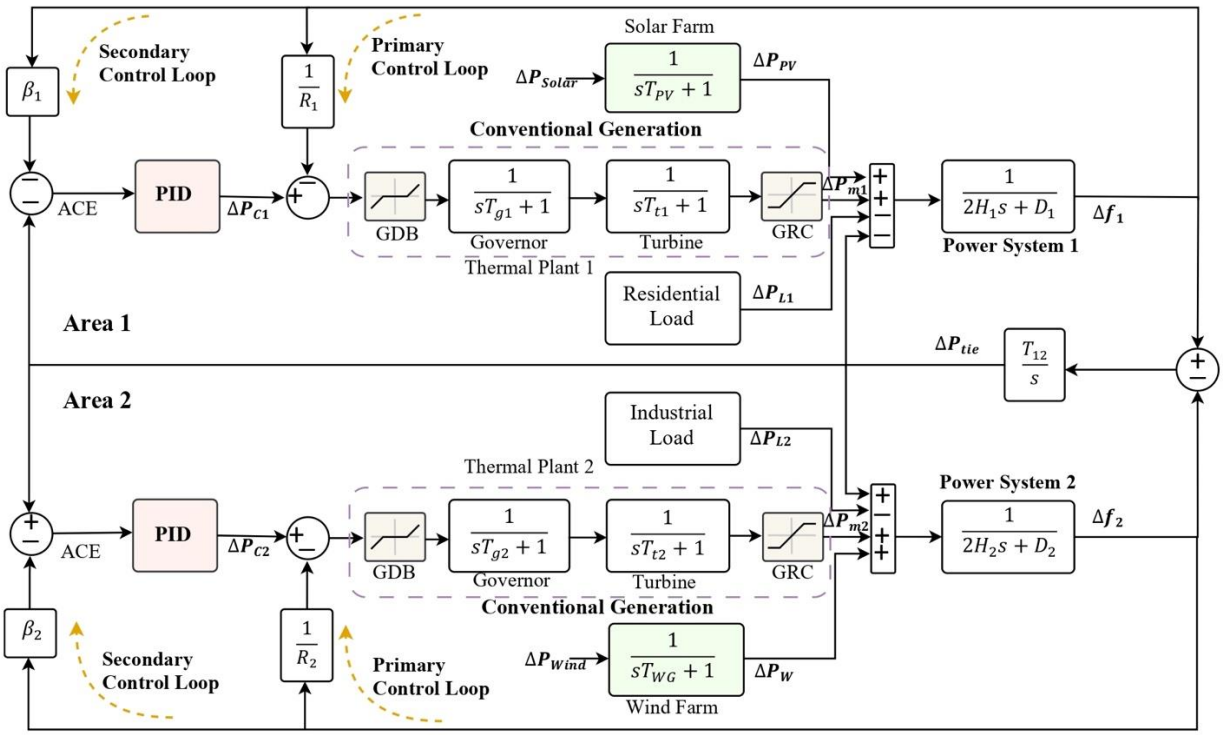

Fig. I.17: (AGC) of a two-area power system with two different renewable energy sources

I.10. Low Inertia

The concept of power system inertia is closely tied to the stored energy within the spinning masses interconnected within the power grid. It characterizes the duration over which this stored energy can sustain the total rated power supply. This energy reservoir is fundamental to power system dynamics. In the context of an individual generator, it is determined by factors such as the moment of inertia of its spinning mass, denoted by *J*, and its rotational velocity. According to basic physics principles, the moment of inertia of a spinning mass can be computed from the ratio of its stored kinetic energy to the square of its rated velocity. Although the rotational speed of a generator's spinning mass fluctuates around a nominal speed, denoted as ω_r, for analytical purposes, it is commonly assumed to maintain this nominal speed consistently [26].

This assumption facilitates the redefinition of inertia using the inertia constant, H, expressed as:

$$H = \frac{E_{kinetic}}{S} \tag{I.20}$$

Where $E_{kinetic} = \frac{1}{2} J{\omega_n}^2$, *J* represents the moment of inertia (kgm^2), ω denotes the rotor speed (*rad/s*), *Te* and Tm represent the electrical and mechanical torque respectively. *Pe* and *Pm* represent the electrical and mechanical power respectively, and *S* is the system rated power (VA).

By normalizing the inertia constant of each generator based on the same rated power, the total inertia constant can be determined by summing each individual constant. The influence of inertia on frequency behavior can be likened to a spring: a stiffer spring corresponds to higher inertia, and conversely [26]**.**

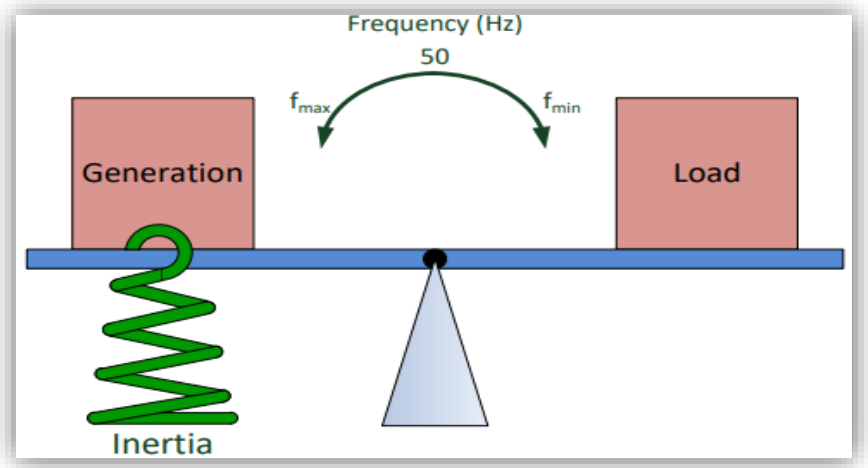

Fig. I.18: The Relationship Between Inertia, Generation and Load

I.10.1. The Effect of Low Inertia

The effect of low inertia in a power system is profound, impacting its operational dynamics and stability margins. In particular, the response of rotating machines, inherent to inertia, diminishes with the increasing integration of inverter-connected Renewable Energy Sources (RES). The level of inertia dictates the rate of frequency deviation in the initial seconds following a disturbance, hence lower inertia leads to swifter frequency changes. Consequently, the operation of primary frequency control and protection systems becomes more intricate, given the larger and faster transient frequency deviations [27].

I.11.Conclusion

The initial section of this memoir provides a concise overview of automatic generation power systems for simulation purposes. Additionally, various types of constraints have been discussed to enhance realism in studies. Lastly, the impact of Renewable Energy Sources (RESs) on the power system, along with some RESs models, has been examined.

Chapter II: Virtual Rotor Control Based EV

II.1. Introduction

As the energy landscape shifts towards renewable sources, maintaining grid stability poses significant challenges due to the lack of inherent inertia in wind and solar power. This chapter explores advanced concepts in virtual rotor control (VRC), which emulates the inertial response of traditional generators using power electronics and control algorithms. Key topics include derivative techniques for simultaneous inertia and damping emulation, frequency regulation, and measurement delay using phase-locked loops (PLLs). Additionally, it discusses the role of electric vehicles (EVs) in providing virtual inertia and introduces the Zebra Optimization Algorithm (ZOA) for optimizing all parameters of the system, ensuring efficient and stable grid operation in the renewable energy era.

II.2. Frequency Regulation in Regards to Inertia Control

Frequency stability is a critical concern in micro grid design, operation, and control, primarily stemming from imbalances between load consumption and power generation. In traditional power systems, specifically synchronous generator-based systems, the inherent inertia and damping properties from the rotor of synchronous generators play a crucial role in maintaining frequency stability during contingencies such as RES variations or changes in load. This relationship, encompassing generated power, load power, system inertia, system damping, and frequency deviation.

To maintain frequency stability at a consistent nominal value (e.g., 50 or 60 Hz) across a wide range of micro grid operations, three primary control units are typically utilized:

1. Inertia (Initial) Control

2. Primary Control

3. Secondary Control

These control units are specifically designed to address contingencies, as illustrated in Fig II.1. For a comprehensive understanding of these control processes. Focusing on the inertia

response, the stored inertia power (kinetic energy) within the rotors of synchronous generators works to counteract imbalances through inertia control, typically before primary control becomes fully active. The relationship between the inertia of the synchronous generator and the microgrid's overall inertia can be determined as follows [30, 15]:

$$H = \sum_{i} (H_{SGi} S_{SGi}) / S_{MG} \qquad (II.1)$$

Where S_{SGi} means the rated power of the synchronous generator, and S_{MG} means the rated microgrid power.

Recently, in microgrids, the synchronous generators have been replaced by inverter/converter-based Renewable Energy Sources (RESs). Hence, the response of system inertia (*H*) and system damping (*D*), typically during 1-10s, is significantly decreased. Accordingly, the rate of change of frequency or derivative of frequency (*df/dt*) of the microgrids increases, leading to rapid frequency deviation, larger frequency drop/dip, system instability, and in the worst case; a rapidly cascading failure or power blackout. It is noted that during the short time interval of 1-10s, the primary and secondary control units are not effective enough to counteract the contingency especially under the severe situations of low system inertia and damping caused by RESs penetration [17].

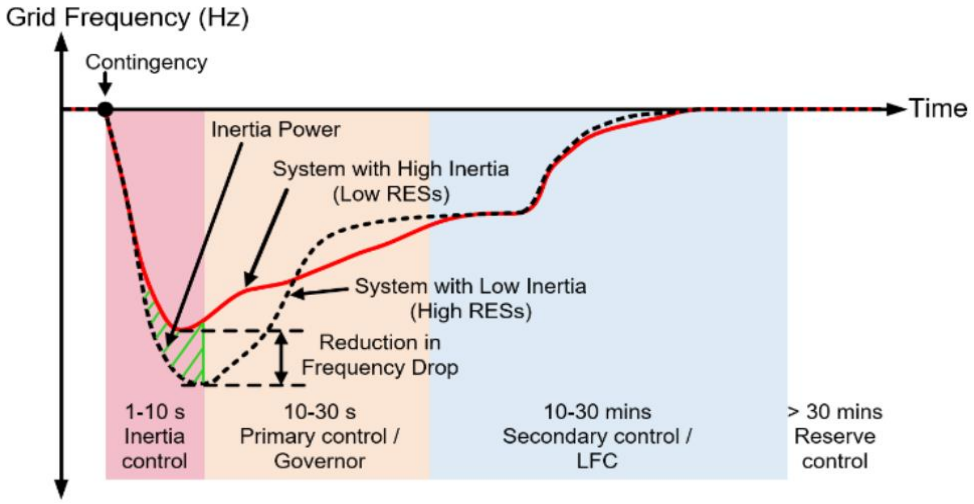

Fig II.1: Time intervals of frequency response during a contingency.

II.3. Concept of Virtual Inertia Control

The idea of emulating control of virtual inertia is utilized to create damping and inertia features derived from traditional synchronous generation, bolstering system inertia stability and enabling increased penetration of Renewable Energy Sources (RESs) in frequency management. In this work, the assumption is made that emulating inertia power is achievable by integrating an energy storage system (ESS), power converter, and control methodology. Consequently, the ESS functions as an inertial component, capable of adjusting system active power and regulating frequency through an inertia response facilitated by modifying the control attributes of the relevant power converter. It's noted that the rate of change of frequency (ROCOF) is influenced by system inertia and initial power discrepancies. Thus, ROCOF is calculated as follows: is

$$\frac{d\omega}{dt} = \frac{\omega^2(T_m - T_e)}{2HS} \qquad (II.2)$$

The ROCOF can be represented in form of per unit (p.u.) as follows:

$$\frac{d\omega}{dt} = \frac{P_m - P_e}{2HS} \qquad (II.3)$$

In this work, the pivotal aspect of inertia control lies in the derivative control technique, enabling the determination of the ROCOF for adjusting the additional active power to the system's set-point value post-disturbance or RES integration. To accurately model the ESS's behavior, a low-pass filter is introduced into the system, ensuring a dynamic response. This filter, of the low-pass type, also addresses the noise interference stemming from frequency measurements, a concern given the sensitivity of derivative control to such noise. Furthermore, a limiter block is employed to confine the minimum and maximum power capabilities of the ESS, reflecting its real-world energy constraints [27].

ESS deployment has taken different physical forms, finding applications directly within frequency-response services to aid in managing ROCOF during frequency events. Over the past decade, ESSs have emerged as vital elements in integrating renewable energy sources due

to their ability to provide frequency stability and balance, potentially enhancing future dispatch operations [28].

The simplified EV model can be represented as follows:

$$G(s) = \frac{1}{1 + sT_{VI,\ i}} \tag{II.4}$$

Therefore, the dynamic equation for imitating virtual inertia power is evaluated using:

$$\Delta P_{inertia} = \frac{K_{VI,\ i}}{1 + sT_{VI,\ i}} \left[\frac{d(\Delta fi)}{dt}\right] \tag{II.5}$$

In this context, K_{VI} refers to the virtual inertia constant, T_{VI} represents the virtual inertia time constant of the added filter used to mimic the dynamic behavior of the ESS, and Δf denotes the system frequency deviation.

II.4. Virtual Rotor Control

This section elaborates on a pioneering approach that leverages derivative techniques for virtual inertia control, aiming to concurrently emulate virtual inertia and damping. The integration of these aspects is crucial for significantly enhancing frequency performance and mitigating system instability risks arising from inadequate damping and inertia [28].

II.4.1. Design Objective: Simultaneous Virtual Damping and Inertia Support

The primary design goal of this innovative strategy is to provide simultaneous support for virtual damping and virtual inertia. This is particularly pertinent for bolstering conventional synchronous generators, especially in environments with low system inertia and damping due to the substantial penetration of RESs within microgrids.

II.4.2. Integrated Components and Dynamic Modeling and Operational Functionality

This conceptual framework seamlessly integrates various components, including short-term ESS, inverters, and a sophisticated inertia control technique. Notably, this control technique operates independently of primary and secondary control units, thereby ensuring optimal utilization of ESS energy to enhance system frequency stability across both steady-state and transient conditions [28, 29].

Fig. II.2. illustrates the dynamic modeling of this novel technique, encompassing the virtual inertia component and its utilization of inertia emulation technology via the derivative technique. This methodology precisely determines the rate of frequency change (df/dt) to facilitate accurate adjustments to added power during microgrid contingencies. Simultaneously, the virtual damping component rapidly stabilizes based on system frequency deviations, proportionally controlling active power through the inverter-based ESS for swift and precise adjustments [30].

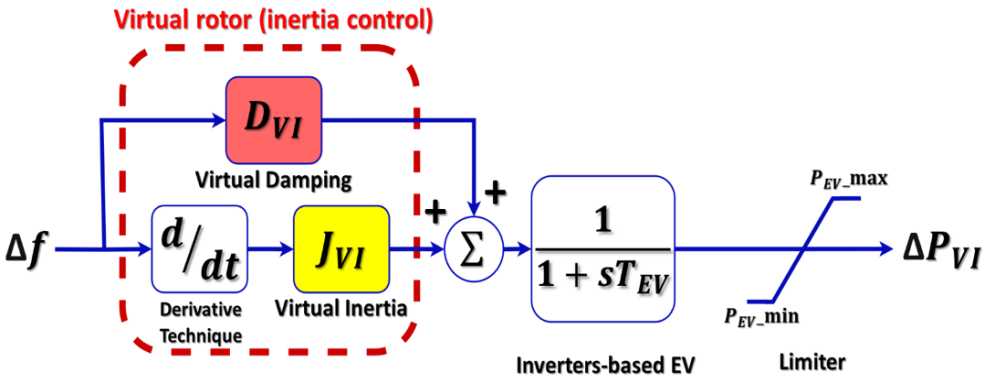

Fig II.2: The dynamic structure of derivative technique-based virtual inertia control to imitate virtual damping and inertia.

II.4.3. Performance Benefits and Comparative Advantage

The proposed virtual inertia control solution offers a multitude of performance benefits, outshining conventional control methods in several key aspects:

- *Enhanced System Stability:* By concurrently emulating virtual inertia and damping, the system significantly enhances overall stability, especially in low inertia and damping scenarios. This results in smoother frequency response and minimizes the risk of system instability or collapse, ultimately improving grid reliability.

- *Improved Frequency Regulation*: Precise adjustment of added power based on df/dt allows for fine-tuned frequency regulation, even during sudden contingencies or fluctuations. This capability ensures optimal frequency levels, enhancing grid performance and operational efficiency.
- *Adaptive Control Mechanism:* Operating independently of primary and secondary control units, the system responds swiftly and autonomously to varying grid conditions. This adaptability ensures optimal performance under diverse circumstances, contributing to overall grid stability and reliability.

In summary, the proposed virtual inertia control solution offers a comprehensive suite of performance benefits and represents a significant advancement in grid stability and reliability, setting a new standard in control system efficiency and adaptability.

II.5. Virtual Rotor Control Based EV with PLL Effect

This study introduces VRC to enhance microgrid stability and accommodate a significant proportion of Renewable Energy Sources (RESs) in the microgrid. The concept is elucidated through EVs. The control strategy employed in this study is the derivative control technique, which adjusts the output power of the EVs to achieve the desired response from the microgrid when a disturbance occurs. This is achieved by virtually emulating the inertia and damping properties of the synchronous generator [31]. The general equation for emulating the inertia and damping of the system can be demonstrated as follows:

$$\Delta P_{imitate} = K_{VI}\left[\frac{d\Delta f_{PLL}}{dt}\right] + K_{VD}(\Delta f_{PLL}) \qquad (II.6)$$

Where: K_{VI} is the virtual inertia constant and K_{VD} denotes the virtual damping constant. $\Delta P_{imitate}$ is the variation in the active power of the converter/inverter.

II.5.1. PLL Measurement Delay

A phase-locked loop (PLL) is a closed-loop system in which an internal oscillator is controlled to keep the time of some external periodical signal by using the feedback loop [32].

The PLL techniques are broadly used in fields like communications, computers and modern electronics. They can generate stable frequencies synchronized with external periodical events, recover relevant signals from distorted sources or distribute clock-timing pulses in complex control systems [33].

PLL is crucial in power electronics-based converters/inverters as it serves to measure frequency and synchronize with the grid. Given that VRC involves converters, it relies on PLL for swift responses to changes in microgrid frequency. Consequently, VRC's effectiveness in handling rapid frequency variations hinges on PLL performance.

However, PLL dynamics can introduce time delays, noises, and oscillations to the system. Therefore, it's vital to consider these effects when designing frequency control mechanisms. The action of PLL, including the measurement of time delay, can be modeled using a first-order model. The dynamic configuration of PLL with measurement delay encompasses a phase detector, loop filter, and voltage-controlled oscillator, illustrated in Fig II.3.

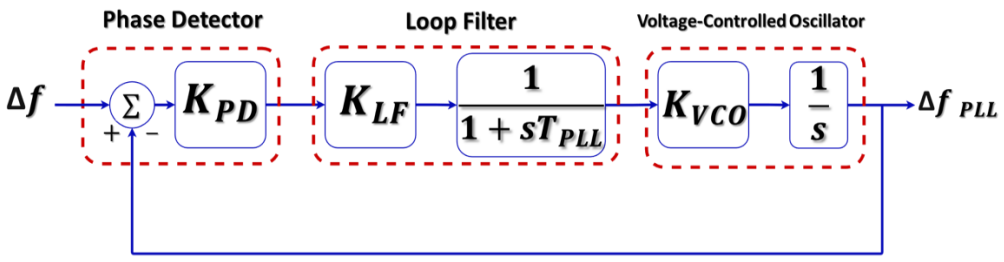

Fig II.3: Dynamic model of PLL measurement delay

Considering $K_{PD} = K_{VCO} = 1$, the second-order dynamic equation or control law of PLL with measurement delay can be obtained as [34]:

$$\Delta f_{PLL} = \frac{K_{LF} \cdot s + \frac{K_{LF}}{T_{PLL}}}{S^2 + K_{LF} \cdot s + \frac{K_{LF}}{T_{PLL}}} \qquad (II.7)$$

In addition, *(II.8)* can be written in the form of a normalized function as:

Where:

The approximated time constant of the PLL transfer function is $\tau = 1/\zeta\omega_n$ for 1 % of steady-state response [35], where, $\omega_n = 1.5$ and $\zeta = 1/\sqrt{2}$. Δf is the system frequency change. K_{PD} is

$$\Delta f_{PLL} = \frac{2\zeta\omega_n \cdot s + \omega_n^2}{S^2 + 2\zeta\omega_n \cdot s + \omega_n^2} \quad (II.8)$$

$$\omega_n = \frac{\sqrt{K_{LF}}}{\sqrt{T_{PLL}}} \quad and \quad \zeta = \frac{\sqrt{K_{LF}T_{PLL}}}{2} \quad (II.9)$$

the phase-detector control gain. K_{LF} is the loopfilter control gain. K_{VCO} is the gain of the voltage-controlled oscillator. T_{PLL} is the time constant of the PLL.

To effectively mitigate the impact of measurement delay, it becomes imperative to implement an additional control alongside VIC. Therefore, the introduction of a PID controller is advocated. This choice is justified by its heightened robustness, broader stability margins, and enhanced adaptability in shaping frequency responses, surpassing the capabilities of its integer-order counterparts.

II.6. Electric Vehicle

Electric vehicles (EVs) have evolved beyond mere modes of transportation, transitioning into integral components of modern energy ecosystems. Within micro-grid operations, their role as adaptable energy storage units has become increasingly significant. This section explores the multifaceted integration of EVs within micro-grid environments, examining their ability to adjust charging and discharging patterns according to grid needs. By leveraging the versatility and cost-effectiveness of EVs, micro-grids stand to benefit from enhanced renewable energy integration and grid stability. This section advocates for the utilization of EVs over traditional energy storage systems within micro-grids, highlighting their tailored suitability for localized energy management. Unlike larger grids where the impact of EVs may be limited, micro-grids derive substantial advantages from the agile nature of EVs, enabling precise adjustments to energy dynamics on a smaller scale. This section delves into the economic, environmental, and

operational benefits of integrating EVs into micro-grid operations, emphasizing their pivotal role in shaping the future of decentralized energy systems [36].

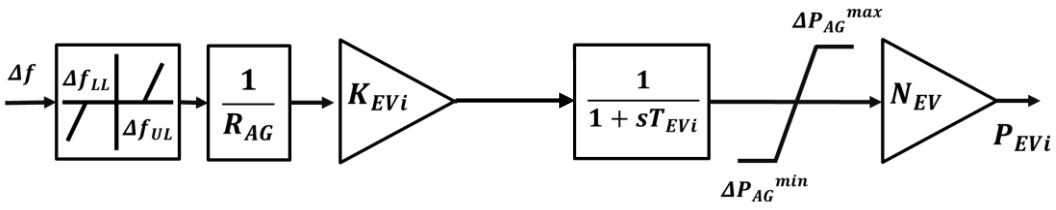

Fig. II.4: The structure of the aggregate EVs model.

In each area, discharged EVs are utilized to mitigate the mismatch that occurs during contract violations. An aggregate model of EV fleets, depicted in Fig. II.4, includes components such as a battery charger, primary frequency control (PFC), the battery charger is responsible for managing the power exchange between the grid and the EV batteries. However, there is a risk that all EVs could suddenly disconnect from the grid, leading to undesired frequency responses. To prevent this, a dead band function with droop characteristics is incorporated into each EV [36].

The dead band limits are crucial for maintaining stability. Additionally, the drop coefficient for the aggregate model R_{AG} is aligned with conventional units.

In Fig. II.4, K_{EVi} represents the EV gain, while T_{EVi} denotes the time constant of the battery. The gain K_{EVi} is dependent on the state of charge (SOC) of the EVs. The variable ΔP_{EVi} indicates the incremental generation change of EVs in area i (in p.u.). The maximum and minimum power output of the EV fleets are denoted by $\Delta {P_{AG}}^{max}$ and $\Delta {P_{AG}}^{min}$, respectively.

This aggregate model ensures that EV fleets can effectively contribute to stabilizing the grid, particularly during periods of imbalance or contract violations. The integration of dead band functions and droop characteristics helps maintain a stable frequency response, even when EVs are rapidly connecting or disconnecting from the grid.

II.6.1. EV Gain (K_{EVi}): Its Role and Importance

The EV gain (K_{EVi}) is a crucial parameter in the integration of EVs into micro-grid operations. It represents the contribution of EVs to load frequency control (LFC) when connected to the grid. The aggregate model of EV fleets, as shown in Fig. II.4, consists of several key components including a battery charger, primary frequency control (PFC), and load frequency

control (LFC). The battery charger manages the power exchange between the grid and the EV battery, ensuring efficient energy flow.

II.6.2. State Of Charge (SOC): Impact on EV Integration

The State of Charge (SOC) of an EV battery is a pivotal factor in determining its effectiveness in load frequency control (LFC). SOC levels influence the value of K_{EVi}, which in turn affects how EVs contribute to grid stability. For lithium-ion (li-ion) batteries, which are commonly used in EVs, the SOC level dictates the participation of EVs in discharge or idle mode operations [36].

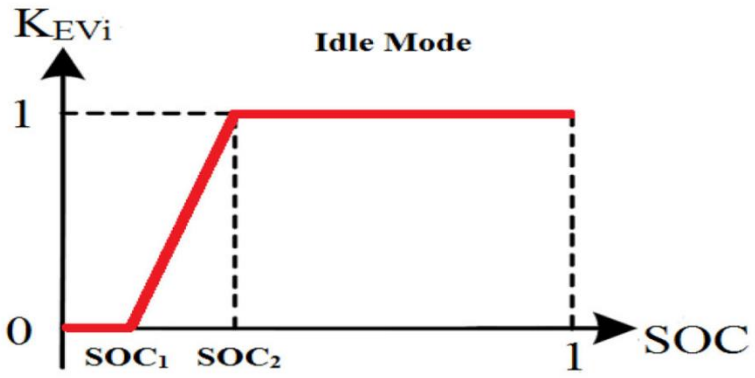

Fig. II.5: K_{EVi} vs. SOC for ideal mode condition.

Fig. II.5 shows the participation of EVs in discharge mode, i.e., idle mode operation as an example. Here, K_{EVi} is always equal to 1 until EV's SOC is less than SOC2. Between SOC1 and SOC2, EV fleets do not participate for LFC fully.

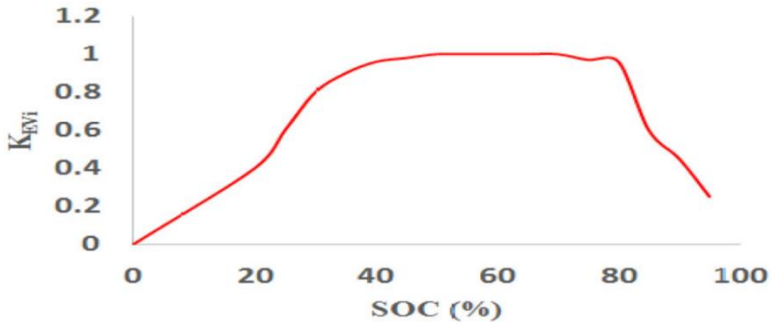

Fig. II.6: K_{EVi} vs. State of charge.

Moreover, Fig. II.6 shows the variation of K_{EVi} with respect to SOC, where K_{EVi} remains at 1 between an SOC of 40% and 80%. Outside this range, the value of K_{EVi} fluctuates, highlighting the variable participation of EVs in grid operations based on their charge levels. This relationship between SOC and K_{EVi} is critical for optimizing the use of EVs in micro-grids [36].

II.7. Proposed Control Strategy

We propose an innovative system to maintain grid stability with the increasing use of renewable energy sources. The system involves measuring the frequency deviation (ΔF) and processing it through a time delay, then a Proportional-Integral-Derivative (PID) controller, and finally a Virtual Rotor Controller (VRC). The system then interacts with electric vehicles (EVs) to provide virtual inertia, resulting in power deviation (ΔP). The EVs help stabilize the frequency by simulating the inertial response of traditional generators. This system demonstrates how advanced control techniques can efficiently achieve grid stability, even with a significant increase in renewable energy sources.

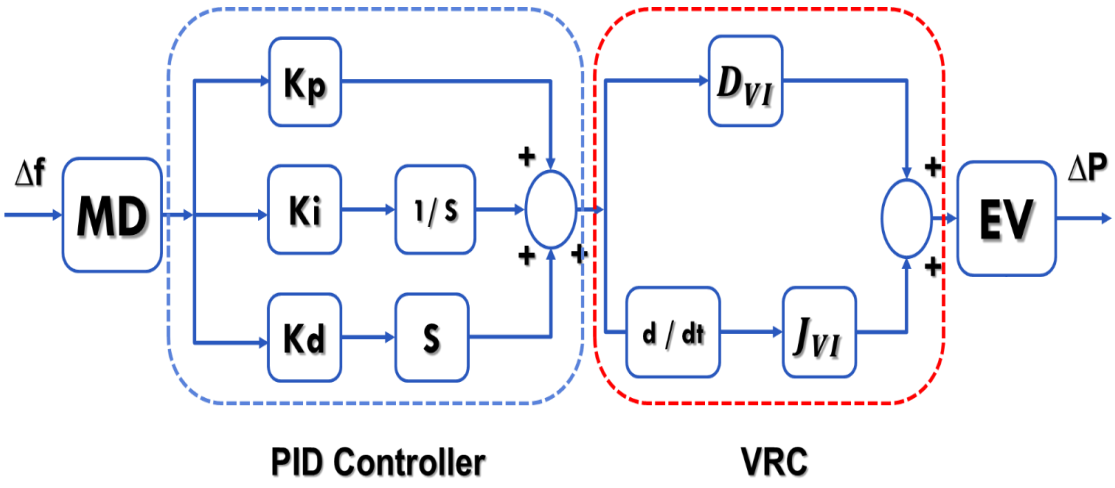

Fig. II.7: Global Controller Scheme

II.8. Optimization

II.8.1. Optimization of Regulator Parameters

In the design and analysis of control systems, some configuration requirements are needed to reduce the system's steady state error. The optimum value of controller parameters is obtained by minimizing a specified objective function. The device synthesis method uses several parameters. (Fig. II.8) flowchart describes the different output parameters used for controller synthesis [37].

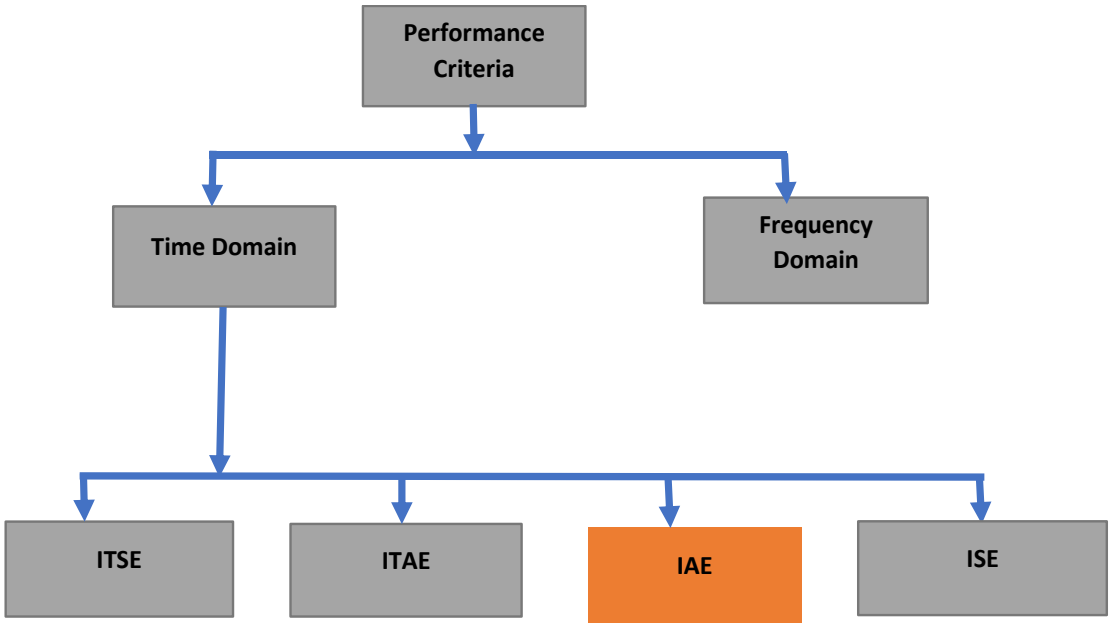

Fig. II.8: Different existing performance criteria

II.8.2. Definition of Standards

a. ITSE

The Integral of Time-Weighted Squared Error (ITSE) is a performance index in control systems that evaluates the error between the desired setpoint and the actual output of the system by weighting the error by time and squaring it. This index gives more weight to errors occurring later, thus encouraging their more effective reduction.
The mathematical equation for ITSE is:

b. ITAE

$$ITSE = \int_0^{\infty} t \cdot e(t)^2 \, dt \qquad (II.10)$$

The Integral of Time-Weighted Absolute Error (ITAE) is a performance index in control systems that measures the error between the desired set point and the actual output by weighting this error by time in an absolute manner. This index emphasizes reducing errors that occur later in the time response, aiming to minimize the error over an extended period.
The mathematical equation for ITAE is

$$ITAE = \int_0^{\infty} t \cdot |e(t)| \, dt \qquad (II.11)$$

c. ISE

The Integral of Squared Error (ISE) is a performance index in control systems that measures the error between the desired setpoint and the actual output of the system by integrating the square of this error over a given period of time. This provides a measure of the sum of squared errors over the entire period, thereby allowing the evaluation of the overall accuracy of the system.

$$ITSE = \int_0^{\infty} e(t)^2 \, dt \qquad (II.12)$$

Where e(t) is the error between the desired setpoint and the actual output at time (t) and $\int_0^{\infty}$ denotes the integral from time 0 to infinity [38].

II.8.3. Proposed Standard

• Integral of the Absolute Error (IAE)

The Integral Absolute Error (IAE) is a performance index in control systems that measures the error between the desired setpoint and the actual output of the system over time. It is useful because it considers the magnitude of the error without regard to its direction, providing a measure of the total accumulated error. This helps evaluate how accurately the system tracks the desired trajectory or maintains the setpoint.

The Integral Absolute Error (IAE) is the suitable performance index examined here and it is presented by:

$$J = IEA = \int_0^{\infty} |e(t)|dt \qquad (II.13)$$

II.8.4 Zebra Optimization Algorithm

The new optimization algorithm ZOA, was developed by Eva Trojovská, Mohammad Dehghani, and Pavel Trojovský. It addresses the challenge of efficiently solving complex optimization problems by drawing inspiration from the foraging and defensive behaviors of zebras. Traditional optimization methods have limitations, leading to the development of metaheuristic algorithms. ZOA falls under this category and is designed to balance exploration and exploitation in search of optimal solutions. While various metaheuristic algorithms exist, the need for new ones arises from the No Free Lunch theorem, which suggests that no single algorithm can solve all optimization problems optimally. ZOA simulates the foraging and defensive behaviors of zebras, leveraging their social dynamics to guide the search for optimal solutions. This unique approach sets ZOA apart from existing algorithms and shows promising results in optimizing both unimodal and multimodal test functions [39].

II.8.5 Mathematical Model

In this subsection, mathematical simulations of zebra's natural behaviors are presented to model ZOA.

a) Initialization

ZOA is a population-based optimizer where zebras represent candidate solutions to an optimization problem. Each zebra's position in the search space determines the values for the

decision variables. The population of zebras is modeled as a matrix, with initial positions randomly assigned.

Each zebra is a candidate solution, and their positions are evaluated using an objective function. The objective function values are compared to determine the quality of the solutions, identifying the best candidate. In minimization problems, the zebra with the least objective function value is the best solution, while in maximization problems, the zebra with the highest value is preferred.

The positions of the zebras and their objective function values are updated in each iteration, identifying the best solution continuously. ZOA updates its members based on two behaviors observed in zebras: foraging and defense strategies against predators, occurring in two different phases during each iteration.

b) PHASE 1: Foraging Behavior

In the first phase, population members are updated based on simulations of zebra behavior when searching for forage. The main diet of zebras is mainly grasses and sedges, but if their favorite foods are scarce, they may also eat buds, fruits, bark, roots, and leaves. Depending on the quality and availability of vegetation, zebras may spend 60–80 percent of their time eating [40]. Among the zebras, there is a zebra called the plains zebra, which is a pioneer grazer, by devouring the canopy of upper and less nutritious grass, provides conditions for other species that need shorter and more nutritious grasses below [41]. In ZOA, the best member of the population is considered as the pioneer zebra and leads other population members towards its position in the search space. Therefore, updating the position of zebras in the foraging phase can be mathematically modeled using (II.14) and (II.15).

$$X_{ij}^{new,P1} = X_{ij} + \ r\ .\ \left(PZ_j - I.X_{ij}\right) \qquad \textit{(II.14)}$$

$$X_{ij}^{new,P1} = \begin{cases} X_{ij}^{new,P1}, & F_{ij}^{new,P1} < F_i\ ; \\ X_i, & else, \end{cases} \qquad \textit{(II.15)}$$

Where $X_i^{new,P1}$ is the new status of the *ith* zebra based on first phase $X_j^{new,P1}$ is its jth dimension value, $F_i^{new,P1}$ is its objective function value, *PZ* is the pioneer zebra which is the best member, *PZj* is its *jth* dimension, *r* is a random number in interval [*0, 1*], *I = round (1 + rand)*, where rand is a random number in the interval [*0, 1*]. Thus, $I \in \{1, 2\}$ and if parameter $I = 2$, then there are much more changes in population movement.

c) PHASE 2: Defense strategies against predators

In the second phase, simulations of the zebra's defense strategy against predator attacks are employed to update the position of population members of ZOA in the search space. The main predators of zebras are lions; however, they are threatened by cheetahs, leopards, wild dogs, brown hyenas, and spotted hyenas [41]. Crocodiles are another predator of zebras when they approach water [41]. Zebras' defense strategy varies depending on the predator. The zebra's defensive strategy against lion attacks is to escape in a zigzag pattern and random sideways turning movements [41]. Zebras are more aggressive against attacks by smaller predators, such as hyenas and dogs, which confuse and frighten the hunter by gathering [41]. In the ZOA design, it is assumed that one of the following two conditions occurs with the same probability:

(*i*) the lion attacks the zebra, and thus, the zebra chooses an escape strategy;

(*ii*) other predators attack the zebra, and the zebra will choose the offensive strategy.

In the first strategy, when the zebras are attacked by lions, the zebras escape from the lion's attack in the vicinity of the situation in which they are located. Therefore, mathematically, this strategy can be modeled using the mode *S1* in (II.16). In the second strategy, when other predators attack one of the zebras, the other zebras in the herd move towards the attacked zebra and try to frighten and confuse the predator by creating a defensive structure. This strategy of zebras is mathematically modeled using the mode *S2* in (II.16). In updating the position of zebras, the new position is accepted for a zebra if it has a better value for the objective function in that new position. This update condition is modeled using (II.17).

$$X_{ij}^{new,P2} = \begin{cases} S1: X_{ij} + R\,.\,(2r-1)\,.\left(1-\frac{t}{T}\right).\,X_{ij}, & Ps \le 0.5\,; \\ S2: X_{ij} + r \cdot \left(AZj - I \cdot X_{ij}\right), & else, \end{cases} \qquad (II.16)$$

$$X_i = \begin{cases} X_{ij}^{new,P2}, & F_{ij}^{new,P2} < F_i \\ X_i, & else, \end{cases} ; \qquad (II.17)$$

where $X_i^{new,P2}$ is the new status of the i th zebra based on second phase, $X_{ij}^{new,P2}$ is its j th dimension value, $F_{ij}^{new,P2}$ is its objective function value, *t* is the iteration contour, *T* is the maximum number of iterations, *R* is the constant number equal to 0.01, *Ps* is the probability of choosing one of two strategies that are randomly generated in the interval [0, 1], *AZ* is the status of attacked zebra, and *AZj* is its *jth* dimension value.

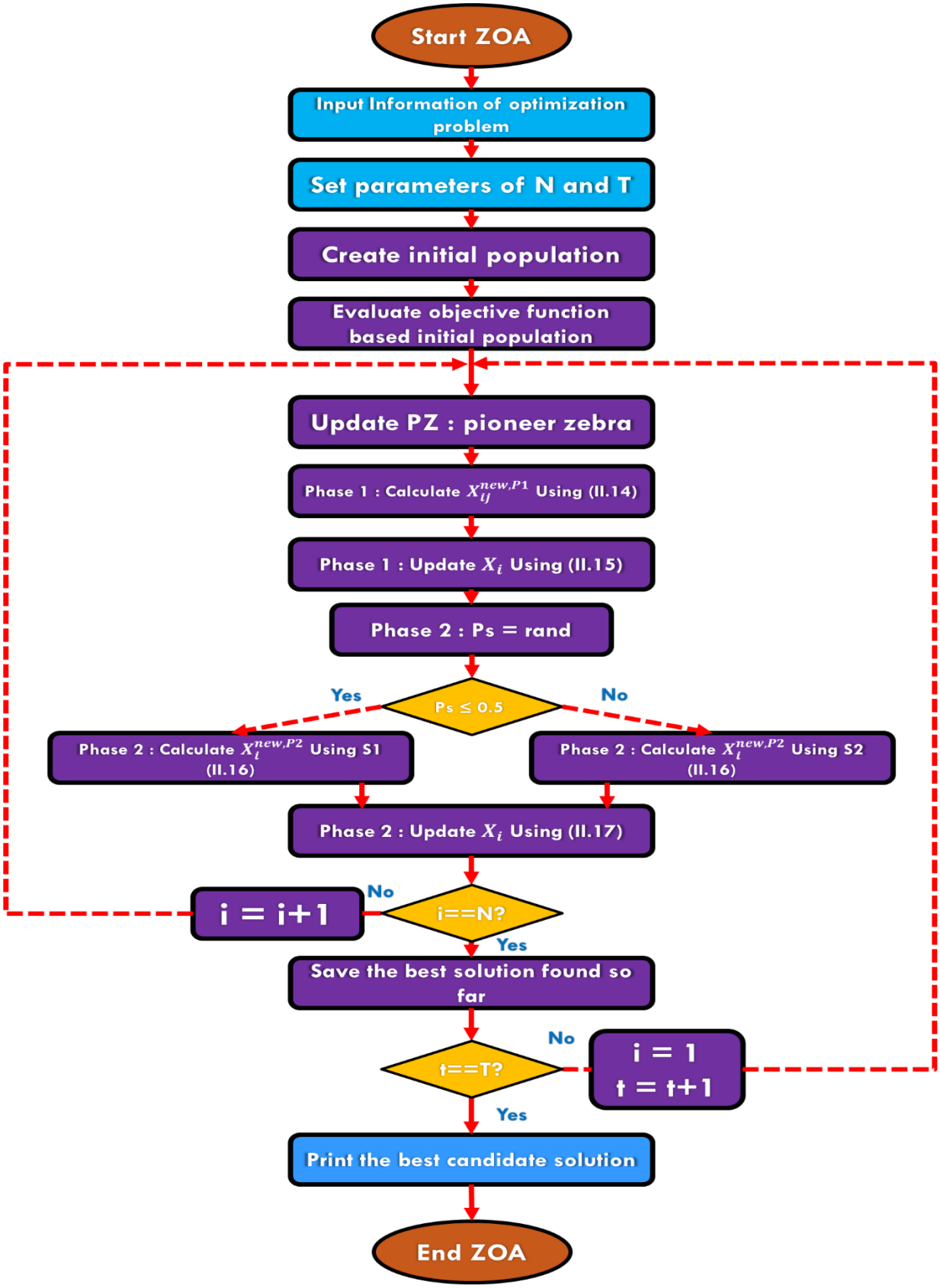

Fig. II.9: Flowchart of ZOA.

II.9. Conclusion

In conclusion, as the energy sector increasingly relies on renewable sources, addressing the challenges of grid stability becomes paramount. This chapter has delved into the innovative field of virtual rotor control (VRC), highlighting its importance in mimicking the inertial response of conventional power systems through sophisticated power electronics and control methodologies. By examining derivative techniques, frequency regulation, and, the chapter underscores the critical advancements required for maintaining grid stability. Furthermore, it emphasizes the potential of electric vehicles (EVs) to contribute to virtual inertia, and introduces the Zebra Optimization Algorithm (ZOA) as a robust tool for optimizing system gains. These insights collectively pave the way for a resilient and efficient grid, capable of supporting the dynamic demands of the renewable energy era.

Chapter III: Simulation and Results

III.1. Introduction

In this chapter, we explore the effectiveness of integrating improved VRC for EVs in an AGC system for a microgrid with RESs. We investigate the impact of inertia on global frequency response without VRC, and then analyze the performance of VRC in providing dynamic responses to the microgrid. A comparative study is conducted to examine the effects of varying measurement delay levels and to analyze its effect. Furthermore, a series of rigorous tests are performed to assess the robustness of the system and demonstrate the potential benefits of VRC with PID in enhancing the overall AGC performance. The optimized settings for LFC and proposed VRC are determined using a novel optimization algorithm called ZOA, which enables us to achieve optimal control strategies for the microgrid.

III.2. Investigated Power System

Our study focuses on a two-area microgrid system, comprising thermal turbines with GDB and GRC, RESs, electric vehicle stations, and domestic loads. The first area is equipped with solar farms, while the second area consists of wind farms. To enhance the stability and performance of the system, we implement VRC in both areas, providing virtual inertia and damping to regulate the output of EVs. Additionally, we consider the measurement delay of PLL in our control strategy. To further improve the VRC performance, we integrate a PID controller to mitigate the effects of measurement delay. The investigated power system is depicted in Fig. III.1, which illustrates the two-area microgrid system with thermal turbines, RESs, electric vehicle stations, and domestic loads. The linearized model of the two-area interconnected thermal power system with RESs is presented in Fig. III.2. Simulations were conducted using MATLAB/SIMULINK with nominal parameters as listed in Table I. The controller parameters were optimized using the ZOA algorithm with 30 populations and 100 iterations, evaluating the IAE criterion. After several tests, the optimum controller parameters were obtained and are presented in Table II. The optimization was performed under a load variation of 0.1 pu in Area 1.

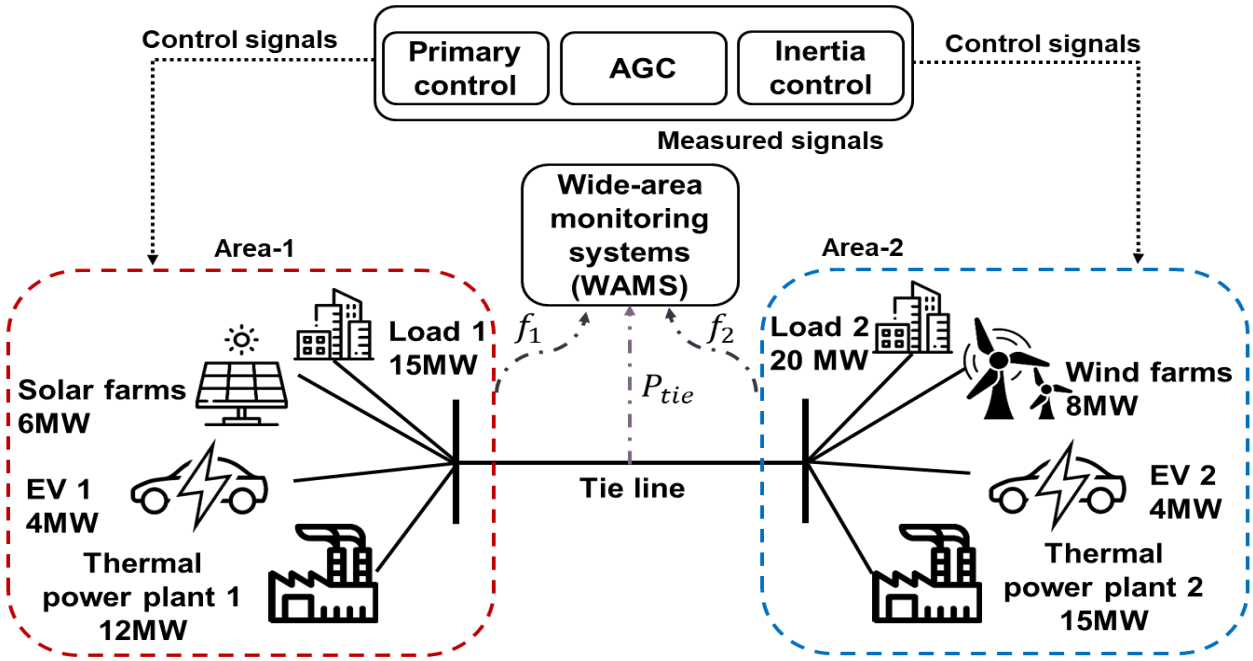

Fig. III.1: Two areas investigated study

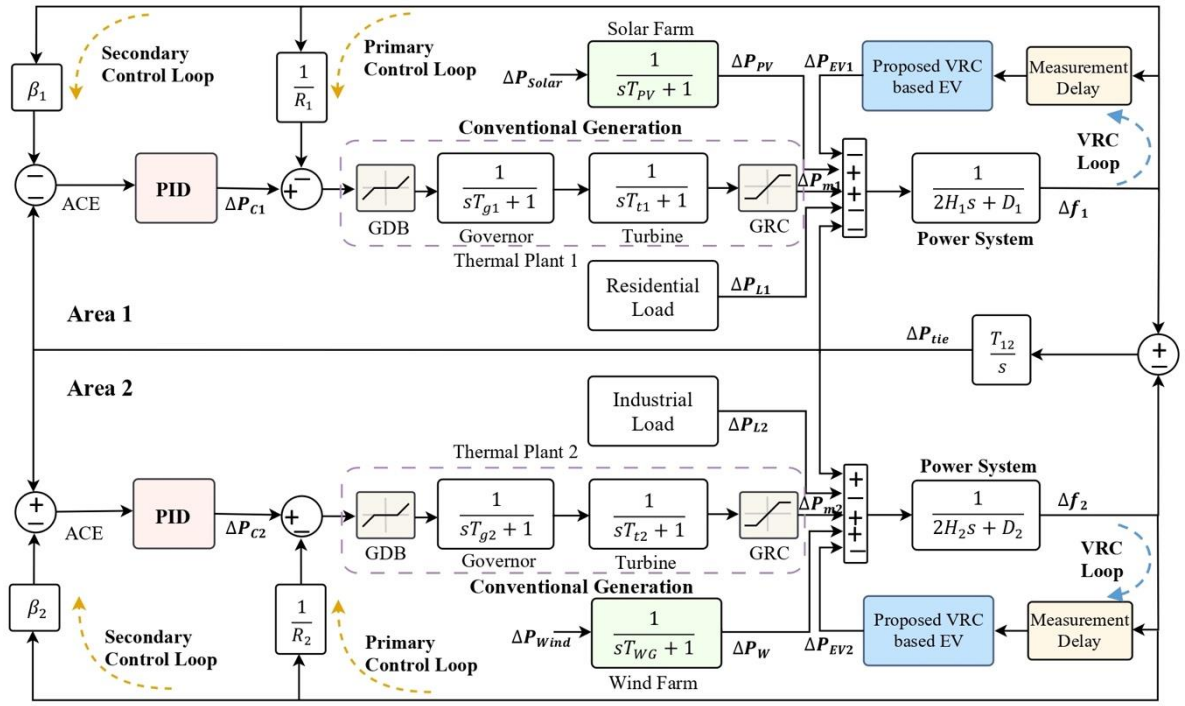

Fig. III.2: Dynamic model of AGC two-area power system with the present of virtual inertia control and PID controller.

Table III.1: Simulation parameters for the MG.

Parameters	***Area-1***	***Area-2***
Frequency bias factor, Bi (p.u.MW/Hz)	0.3483	0.3827
Governor time constant, Tg (s)	0.08	0.06
Turbine time constant, Tt (s)	0.4	0.44
Droop constant, R (Hz/p.u.MW)	3	2.73
System inertia constant, H (p.u.MW s)	0.083	0.1010
Damping coefficient, D (p.u.MW/Hz)	0.015	0.016
Solar system time constant, T_{PV} (s)	1.3	-
Wind time constant, T_{WT} (s)	-	1.5
Maximum limit of valve gate, VU (p.u.MW)	0.5	0.5
Minimum limit of valve gate, VL (p.u.MW)	-0.5	-0.5
System base (MW)	20	
Synchronizing coefficient, T12 (p.u.MW/Hz)	0.54322	
PLL Time constant T_{PLL}	0.943s	
The loop filter control gain K_{LF}	2.12	
EV time constant T_{EV}	0.8	
EV Droop constant R_{AG}	2.4	

Table III.2: Optimal settings of PID_{LFC}, PID_{VRC} and VRC for IAE criterion

Model/ Controller	***Parameter***	***Conventional***	***EV***	***VRC+EV***	***PLL+PID_{VRC}+VRC+EV***
PID_{LFC}	$K_{P,1}$	6.9583	9.9643	9.8696	8.6031
	$K_{I,1}$	6.0596	10	10	9.9994
	$K_{D,1}$	3.221	10	4.5631	3.228
	$K_{P,2}$	6.5856	9.0166	8.9643	6.4339
	$K_{I,2}$	4.6478	8.2955	8.3483	4.3052
	$K_{D,2}$	4.2562	3.3896	4.0295	1.5179
VRC	$J_{I,1}$	-	-	3.0865	5.7843
	$D_{I,1}$	-	-	2.99	1.4905
	$J_{I,2}$	-	-	3.9753	0.8102
	$D_{I,2}$	-	-	2.0124	0.5855
PID_{VRC}	$Kv_{P,1}$	-	-	-	1.0630
	$Kv_{I,1}$	-	-	-	0.6365
	$Kv_{D,1}$	-	-	-	0.8102
	$Kv_{P,2}$	-	-	-	9.5855
	$Kv_{I,2}$	-	-	-	6.0630
	$Kv_{D,2}$	-	-	-	0.6365

III.3.1. The impact of PLL on VRC

In this section, we investigate the impact of measurement delay on the system's performance and stability. To achieve this, we modify the natural frequency ω_n from 2 to 4, while considering two scenarios: *H=50%* and *H=100%*. We utilize the same PID controller parameter values as listed in Table III.1 for the IAE criterion. This experiment simulates the effect of a PLL with measurement delay on the microgrid's response to a 10% load change (0.1 p.u.) in areas 1 and 2. The results are presented in Fig. III. 3 and Fig. III. 4, which show the frequency and EV power response curves.

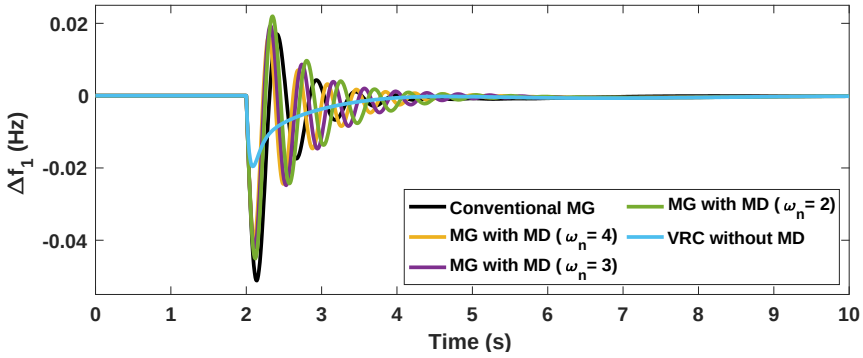

(a)

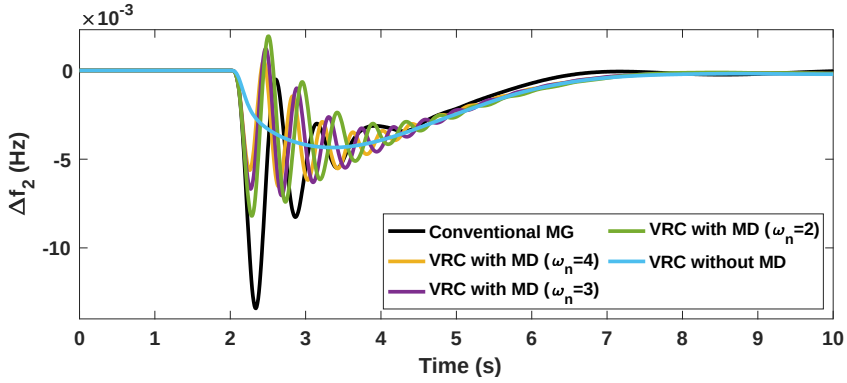

(b)

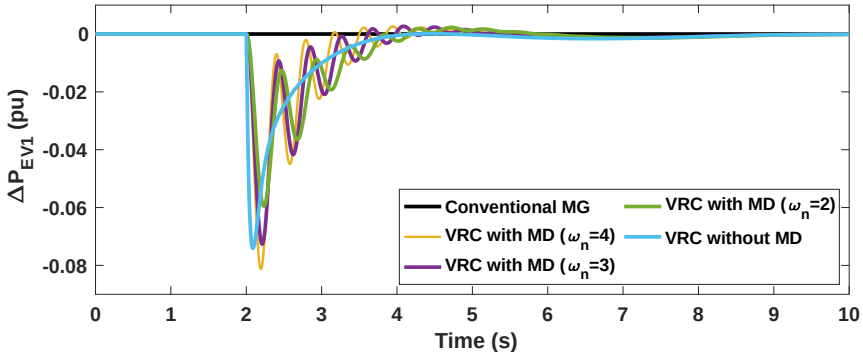

(c)

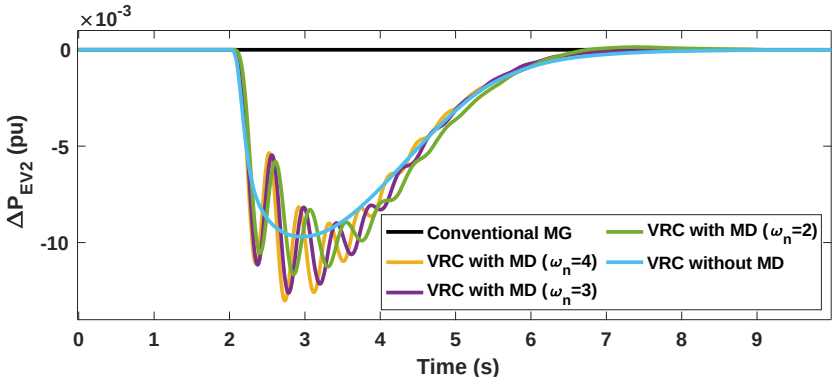

(d)

Fig. III.3: Frequency and EV power response for H=100% (a): Frequency response in area 1, (b): Frequency response in area 2, (c): EV power response in area 1, (d): EV power response in area 2

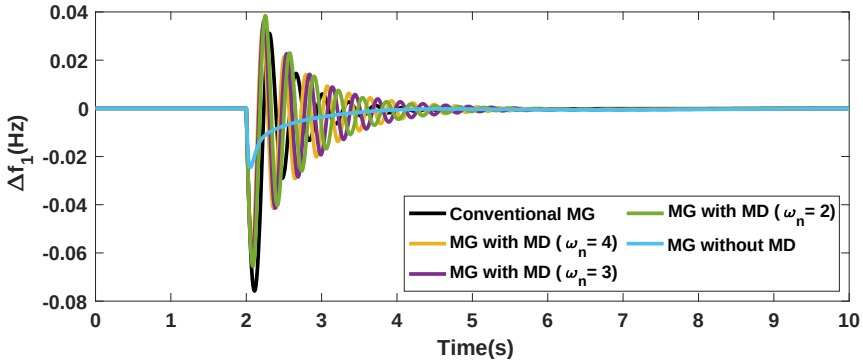

(a)

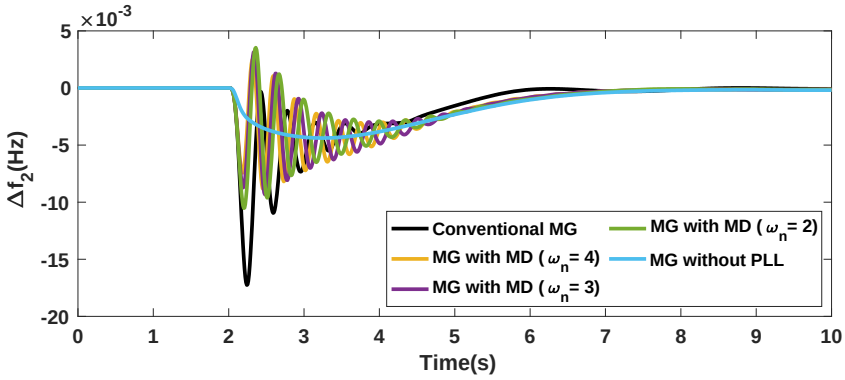

(b)

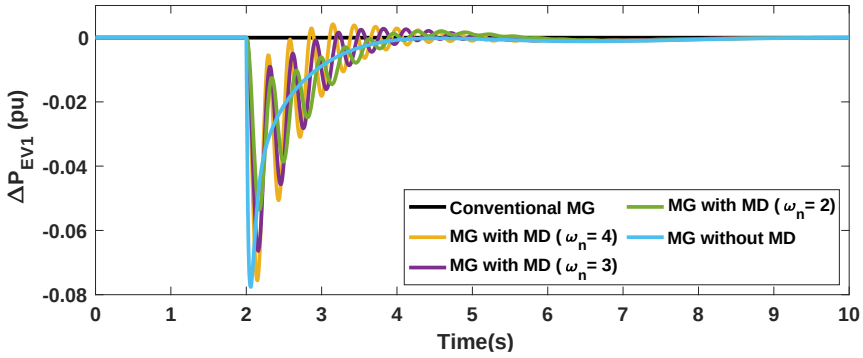

(c)

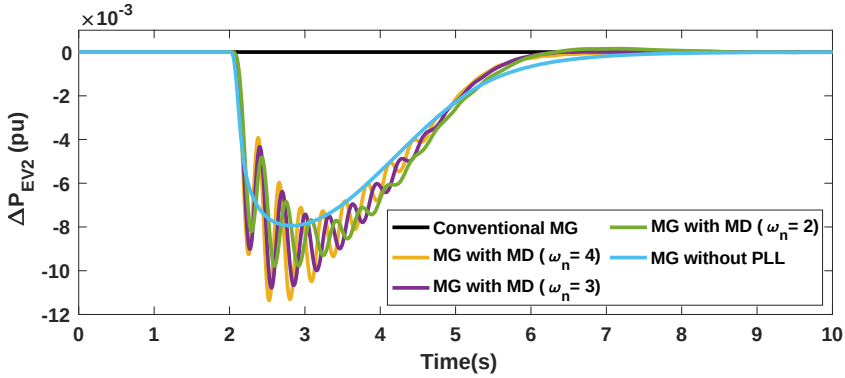

(d)

Fig. III.4: Frequency and EV power response for H=50% (a): Frequency response in area 1, (b): Frequency response in area 2, (c): EV power response in area 1, (d): EV power response in area 2

During the normal operating condition (high system inertia) as shown in Fig. III. 3 the use of the PLL clearly impacts the stability of the microgrid, causing a larger frequency overshoot with severe oscillations. This effect is significantly exacerbated in the low inertia condition, as shown in Fig. III. 4.

However, the effect of the PLL on VRC can be illustrated through the PLL time response. It is evident that when the PLL time constant is low (high ωn), the actual effect of virtual inertia control can be observed. However, when the PLL time constant increases (low ωn), the effect of virtual inertia control is significantly diminished, leading to a deterioration in frequency stability.

III.3.2. Step Load Change

In this section, a comprehensive comparison is conducted to evaluate the performance of the proposed interconnected microgrid under various scenarios. Specifically, the microgrid is simulated without EV, with only EVs, with VRC to control the EVs, and finally with the proposed controller. All simulations are conducted under low inertia and damping conditions (*H=50%*, *D=80%*). Additionally, it is assumed that all EVs in both areas have a state of charge (SOC) between 50% and 80%, which means that the effective number of EVs participating in the grid is K_{EV}=1. Furthermore, the PLL time constant is set to a high value (ω_n=*2*) to mimic real-world conditions. This comprehensive comparison provides valuable insights into the impact of different scenarios on the performance of the proposed interconnected microgrid.

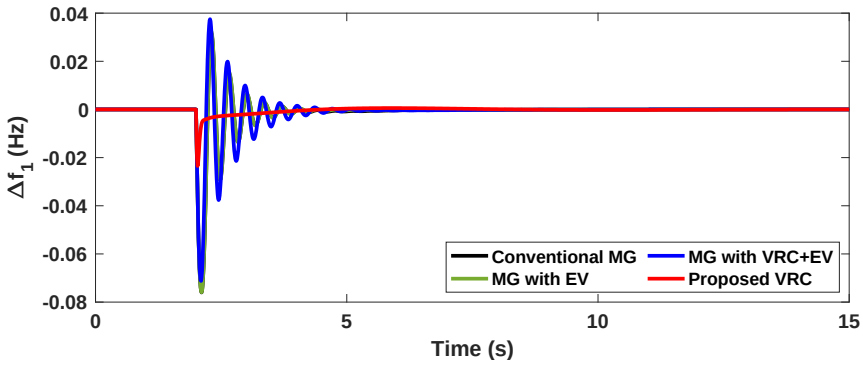

(a)

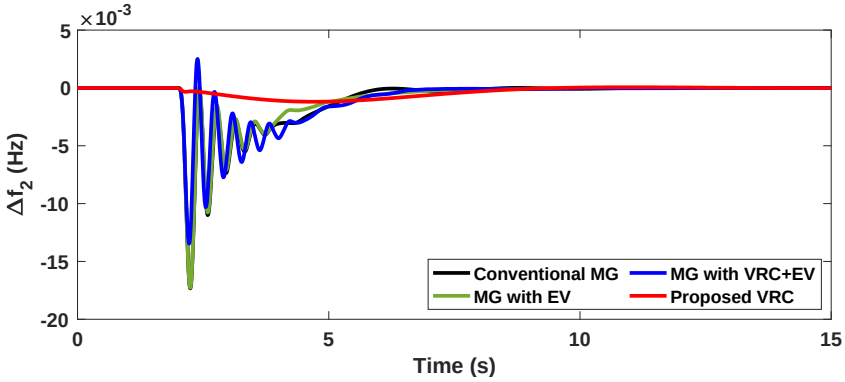

(b)

Fig. III.5. Frequency response under step load change, (a): Frequency response in area 1, (b): Frequency response in area 2

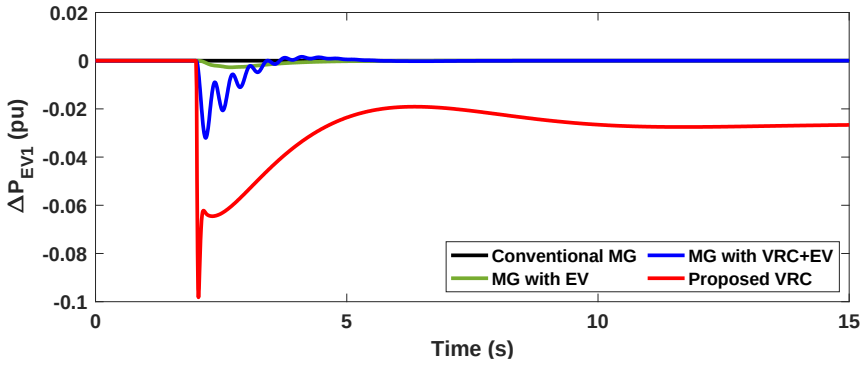

(a)

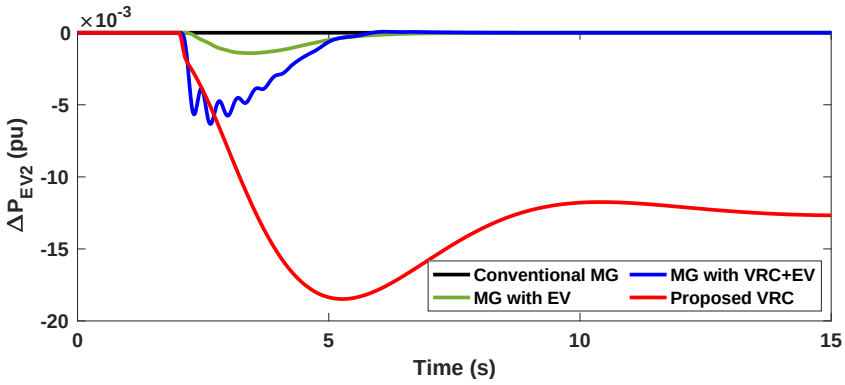

(b)

Fig. III.6: EV power response under step load change, (a): EV power response in area 1, (b): EV power response in area 2

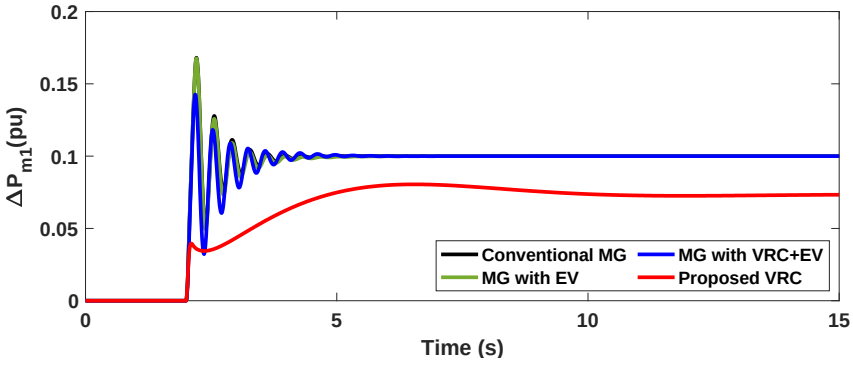

(a)

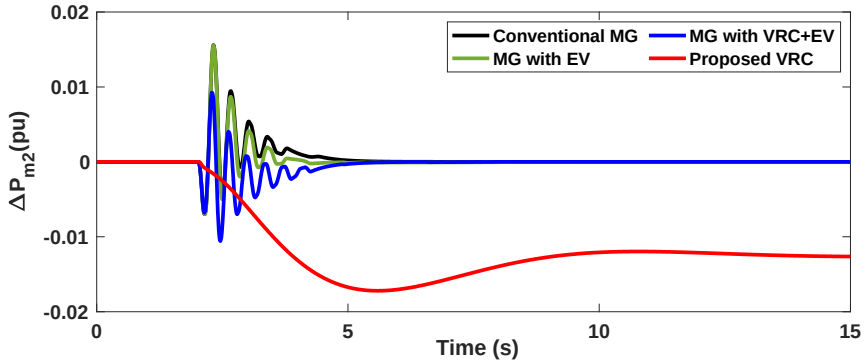

(b)

Fig. III.7: Mechanical power response under step load change, (a): Mechanical power response in area 1, (b): Mechanical power response in area 2

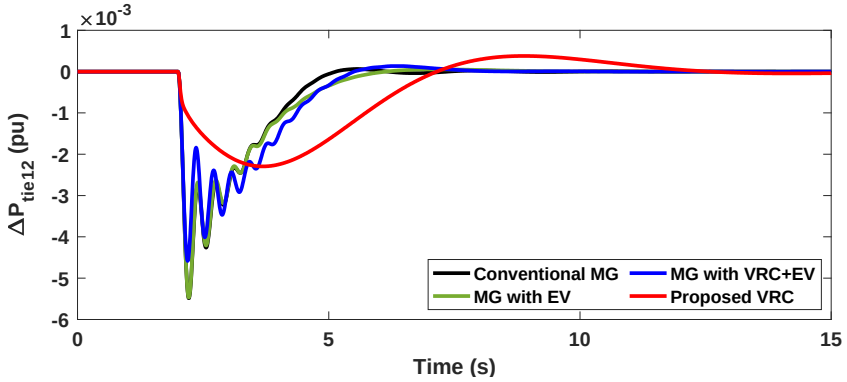

Fig. III.8: Tie-line power response under step load change

The integration of VRC units (EV, VRC, and Proposed) into a system with high levels of RES penetration has resulted in significant improvements in all dynamic responses of the interconnected microgrid. The figures show that the addition of EV, VRC, and Proposed units have collectively improved the frequency response, power output, and power sharing between the generator and EV.

As shown in Fig. III.5, the EV alone had a limited impact on the frequency response, resulting in only a slight improvement. However, when the VRC was implemented, the frequency response improved significantly, although the measurement delay effect still had a noticeable impact. The addition of a PID controller to the VRC with PLL effect effectively mitigated the measurement delay effect, leading to a substantial improvement in frequency response.

Fig. III.6 illustrates the power output of EV, which shows that the proposed method has successfully pushed the EV to provide the necessary power to improve the frequency response. However, it also reveals a static error caused by integrating PID controllers into this VRC.

Fig. III.7 presents a clear picture of power sharing between the generator and EV. The static error caused by the EV has resulted in a lower mechanical power output, which in turn allows the turbine to provide less power.

Overall, the integration of VRC units has been shown to be effective in improving the performance of the microgrid, particularly in terms of frequency response and power sharing. However, there are some limitations and challenges associated with integrating these systems, such as measurement delay effects and static errors.

III.3.3. MG Performance under Random RES Generation and Load Disturbances

To evaluate the robustness of the proposed technique, a more stringent scenario is designed with a lower EV participation rate of K_{EV}=0.8. The microgrid is assessed under the influence of random and varying load disturbances, as well as intermittent disturbances from RESs, as depicted in Fig III.9. The simulation is further challenged by even lower inertia and damping levels, with H=20% and D=50%. This comprehensive testing scenario allows for a thorough evaluation of the proposed technique's resilience and effectiveness in responding to extreme disturbances and uncertainties.

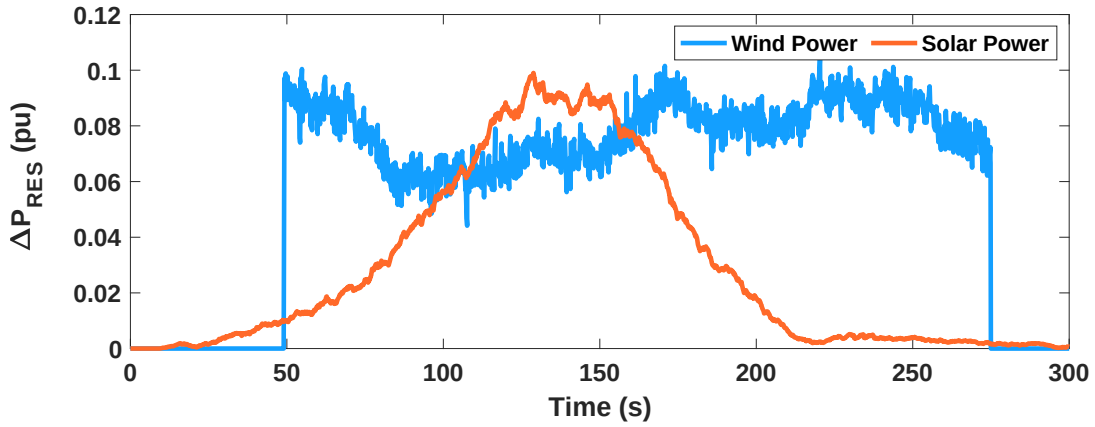

(a)

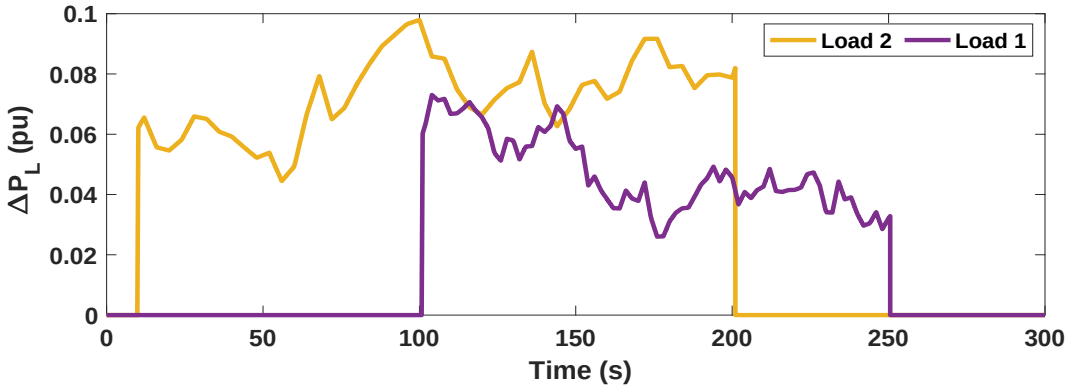

(b)

Fig. III.9: Random disturbances (a): RESs power (b): Load power

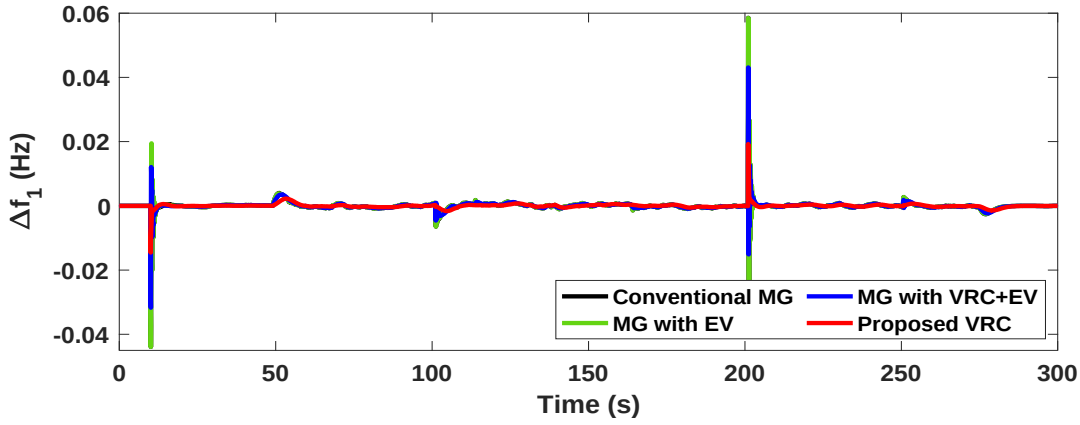

(a)

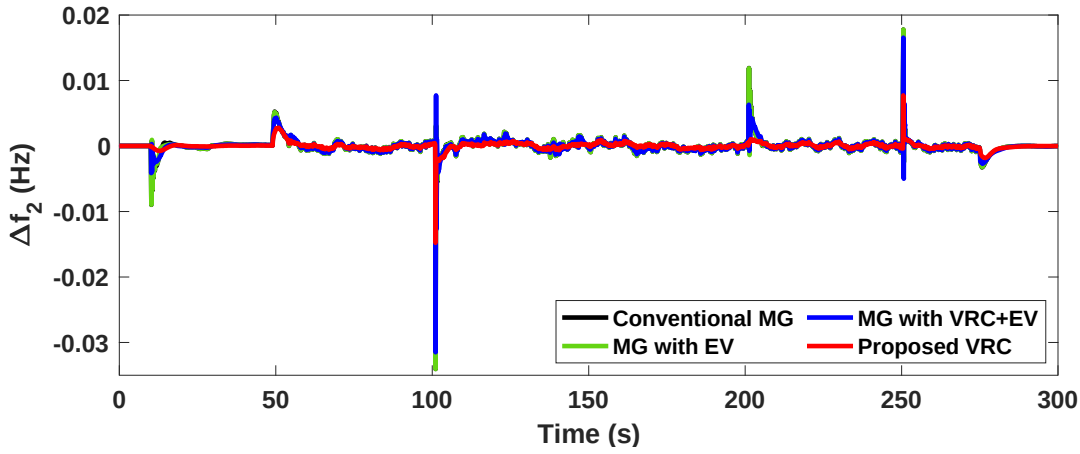

(b)

Fig. III.10: Frequency response under step load change, (a): Frequency response in area 1, (b): Frequency response in area 2

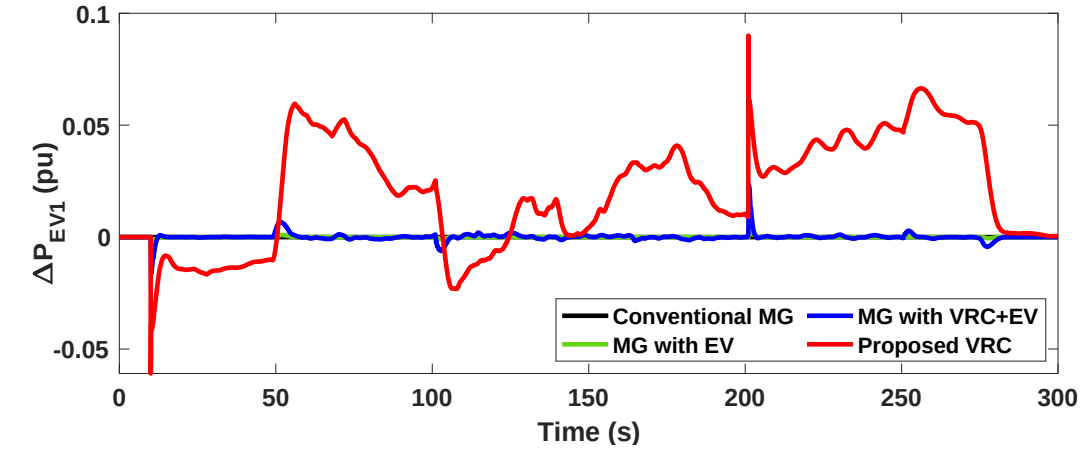

(a)

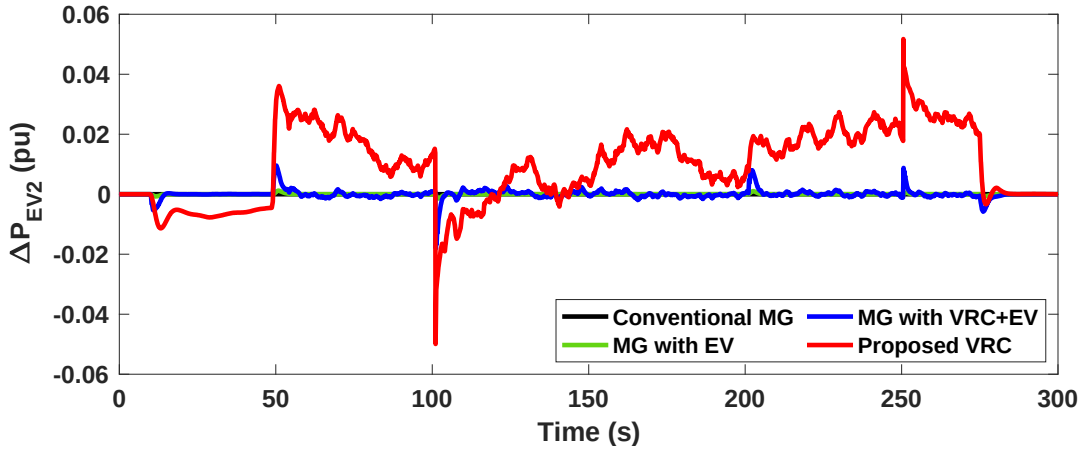

(b)

Fig. III.11: EV power response under step load change, (a): EV power response in area 1, (b): EV power response in area 2

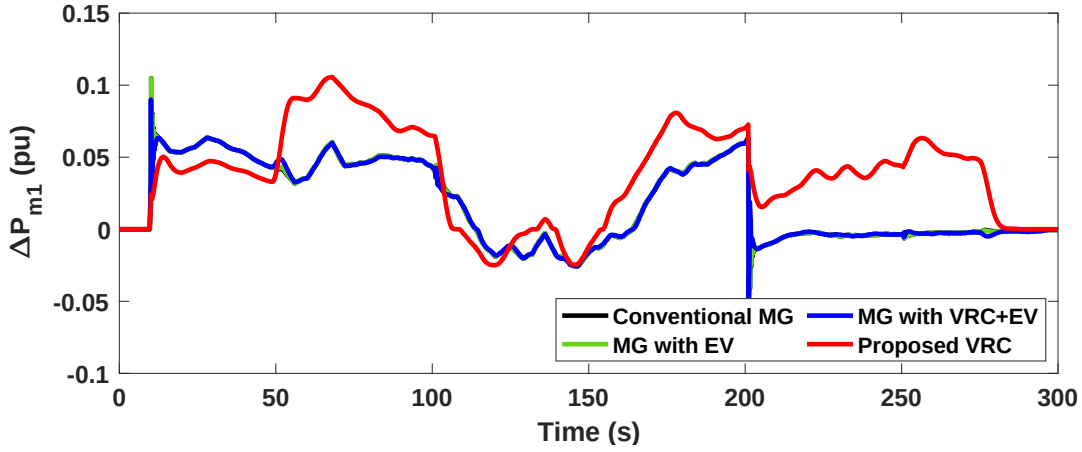

(a)

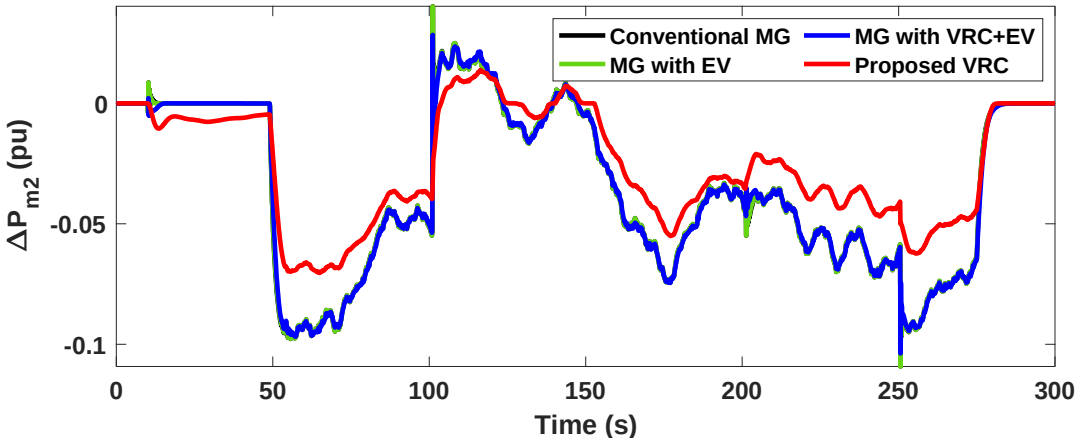

(b)

Fig. III.12: Mechanical power response under step load change, (a): Mechanical power response in area 1, (b): Mechanical power response in area 2

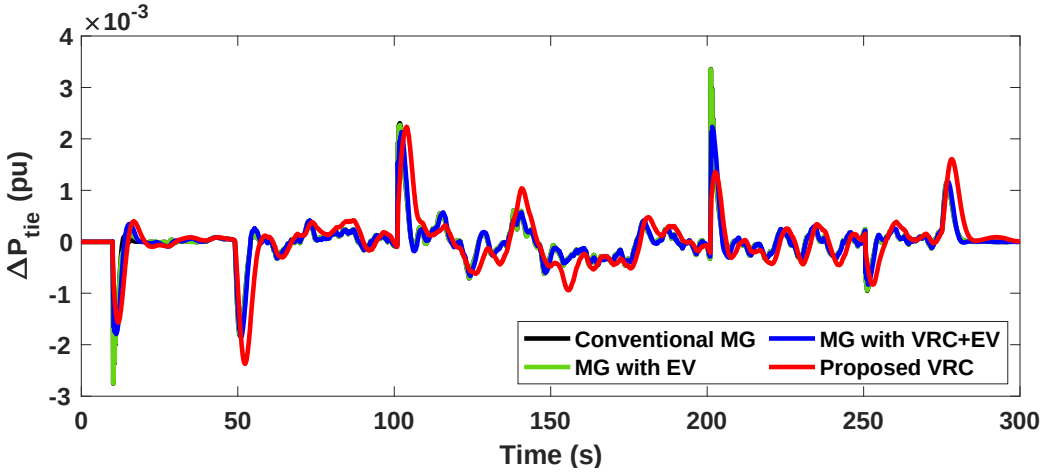

Fig. III.13: Tie-line power response under step load change

As depicted in Fig. III.10, the standalone EV had a limited impact on frequency response, resulting in a marginal improvement. However, when the VRC was introduced, the frequency response exhibited a substantial improvement, although the measurement delay effect still had a noticeable impact. The implementation of a PID controller effectively mitigated the measurement delay effect, leading to a significant enhancement in frequency response.

Fig. III.11 illustrates the power output of EV, which demonstrates that the proposed method has successfully enabled the EV to provide the necessary power to improve frequency response. However, it also reveals a static error caused by integrating PID controllers into this VRC.

Fig. III.12 provides a clear visualization of power sharing between the generator and EV. The static error caused by the EV has resulted in reduced mechanical power output from the turbine, which in turn allows it to supply less power.

In summary, the integration of VRC units has been shown to be effective in improving the performance of the microgrid, particularly with regards to frequency response and power sharing. However, there are some limitations and challenges associated with integrating these systems, such as measurement delay effects and static errors.

III. 4 Conclusion

In this chapter, we demonstrated the effectiveness of using Virtual Inertia Control (VRC), Electric Vehicles (EV), and the new PID proposal in the Automatic Generation Control (AGC) problem. We studied the impact of inertia on frequency response without VRC, EV, and PID. Then, we observed the performance of VRC, EV, and PID, and compared the effect of changing the system's inertia with and without VRC, EV, and PID. Finally, we conducted rigorous tests to determine how VRC, EV, and the new PID proposal can improve the system and enhance its robustness. These tests proved that the proposed control (VRC, EV, and PID) is a reliable solution for the low inertia problem, maintaining the best response even under severe renewable energy source penetrations and random load disturbances.

General Conclusion

This Thesis provides a comprehensive analysis of the challenges and solutions associated with integrating (RESS) into traditional power grids, with a focus on maintaining grid stability amidst the increasing reliance on these sources. The initial sections of the study offered a concise overview of AGC in power systems, introducing various constraints and measurement delays to enhance the realism of simulations. The impact of RESs on the power system was also thoroughly examined, alongside models of these sources.

In response to the critical need for stable and reliable microgrid in the renewable energy era, the concept of Virtual Rotor Control (VRC) was explored. VRC is essential for mimicking the internal response of conventional power systems using advanced electronics and control techniques. *Kev* aspects such as derivative techniques, frequency regulation, and grid synchronization through Phase-Locked Loops (PLLs) were investigated to highlight the necessary advancements for maintaining grid stability.

Additionally, the study emphasized the significant role that Electric Vehicles (EVs) can play in providing virtual inputs, enhancing the stability of power grids. The introduction of the Zebra Optimization Algorithm (ZOA) showcased a robust tool for optimizing system parameters, further contributing to grid resilience.

Extensive tests were conducted to evaluate the performance of the power system under different scenarios. Initially, the impact of PLL time delay on frequency response was studied without the implementation of VRC, EVs, and PID controllers. Subsequent tests incorporated these elements, demonstrating the effectiveness of VRC, EVs, and PID controllers in improving system performance. The comparison highlighted the benefits of changing the system's inertia with and without these control mechanisms.

Rigorous testing confirmed that VRC, EVs, and the new PID proposal, offers a reliable solution to the low inertia problem and measurement delays. These control strategies maintained optimal system response even under severe renewable energy penetrations and random load disturbances, proving their robustness and efficiency.

Finally, after analyzing the results, we found that the good performance was achieved with the system we proposed

This memoir has discussed some important points of control strategies in the low inertia microgrids. For further research, the next suggestions are recommended:

- Develop and implement Model Predictive Control (MPC) strategies for VRC to optimize control actions over a future time horizon.
- Utilize machine learning techniques, particularly neural networks, for maintenance and fault detection in VRC systems and EV batteries.
- Design adaptive control systems that adjust parameters in real-time, implementing algorithms to update control laws continuously and enhance resilience to disturbances.

References

[1] T. Kerdphol, F. S. Rahman, M. Watanabe, Y. Mitani, D. Turschner, and H.-P. Beck, "Enhanced virtual inertia control based on derivative technique to emulate simultaneous inertia and damping properties for microgrid frequency regulation," IEEE Access, vol. 7, pp. 14 422–14 433,

[2] T. Kerdphol, F. S. Rahman, Y. Mitani, K. Hongesombut, and S. Kufeo, "Virtual inertia control-based model predictive control for microgrid frequency stabilization considering high renewable energy integration," Sustainability, vol. 9, no. 5, 2017.

[3] S. Oshnoei, M. R. Aghamohammadi, S. Oshnoei, S. Sahoo, A. Fathollahi, and M. H. Khooban, "A novel virtual inertia control strategy for frequency regulation of islanded microgrid using two-layer multiple model predictive control," Applied Energy, vol. 343, 2023.

[4] S. A. Zaid, A. Bakeer, G. Magdy, H. Albalawi, A. M. Kassem, M. E. El-Shimy, H. AbdelMeguid, and B. Manqarah, "A new intelligent fractional-order load frequency control for interconnected modern power systems with virtual inertia control," Fractal and Fractional, vol. 7, no. 1, 2023.

[5] V. Skiparev, K. Nosrati, A. Tepljakov, E. Petlenkov, Y. Levron, J. Belikov, and J. M. Guerrero, "Virtual inertia control of isolated microgrids using an nn-based VFOPID controller," IEEE Transactions on Sustainable Energy, vol. 14, no. 3, pp. 1558–1568, 2023.

[6] A. Saxena, R. Shankar, O. Al Zaabi, K. Al Hosani, and U. R. Muduli, "Fuzzy rule-based adaptive virtual inertia control for enhancing multi-region micro-grid dynamic response," in 2023 IEEE IAS Global Conference on Renewable Energy and Hydrogen Technologies (GlobConHT), 2023, pp. 1–6.

[7] G. Magdy, H. Ali, and D. Xu, "Effective control of smart hybrid power systems: Cooperation of robust lfc and virtual inertia control systems," CSEE Journal of Power and Energy Systems, vol. 8, no. 6, pp. 1583– 1593, 2022.

[8] H. Abbou, S. Arif, and A. Delassi, "Frequency enhancement of power system with high renewable energy penetration using virtual inertia control based ESS and SMES," in Advanced Computational Techniques for Renewable Energy Systems, M. Hatti, Ed. Springer International Publishing, 2023, pp. 602–613.

[9] K. Hongesombut and R. Keteruksa, "Fractional order based on a flower pollination algorithm PID controller and virtual inertia control for microgrid frequency stabilization," Electric Power Systems Research, vol. 220, p. 109381, 2023.

[10] H. Abubakr, T. H. Mohamed, M. M. Hussein, J. M. Guerrero, and G. Agundis-Tinajero, "Adaptive frequency regulation strategy in multiarea microgrids including renewable energy and electric vehicles supported by virtual inertia," International Journal of Electrical Power & Energy Systems, vol. 129, 2021.

[11] Umashanker, "Modeling of Automatic Generation Control of Thermal Unit," Masters of Engineering in Power System & Electric Drives, Electrical & Instrumentation Engineering Department, Thapar University, Patiala, July 2010.

[12] H. Jahangir, Large Scale Renewable Power Generation, Advances in Technologies for Generation, Transmission and Storage, ISSN 1865-3529

[13] MIHOUBI omar el farouk, BEN DJEMAI Hadj BelKacem " Automatic Generation Control in Low Inertia Power System " Master Thesis , University Amar Telidji - Laghouat

[14] H. Saadat, Power System Analysis McGraw-Hill Series in Electrical and Computer Engineering, 1999.

[15] H. Bervani, Robust Power System Frequency Control. 2th edition, New York Springer Verlag, 2014

[16] Nitesh Thapa, Nilu Murmu, Aditya Narayan, Birju Besra, "Automatic voltage regulator and automatic load frequency control in two-area power system", International Journal of Research in Engineering, Technology and Science, Volume VII, Special Issue, Feb 2017.

[17] P. Kundur, Power System Stability and Control. McGraw-Hill, New York 1994.

[18] A. Halmous, H. Abbou. "Flexible AC Transmission System based Automatic Generation Control," Master thesis, University of Amar Telidji, Laghouat 2020.

[19] Shiroei, M., Toulabi, M. R., & Ranjbar, A. M. "Robust multivariable predictive based load frequency control considering generation rate constraint". International Journal of Electrical Power & Energy Systems, 46, 405-413, 2013.

[20] Bevrani, H., Ghosh, A., & Ledwich, G. (2010). "Renewable energy sources and frequency regulation: survey and new perspectives." IET Renewable Power Generation, 4(5), 438-457.

[21] Sanki, P., Basu, M., & Pal, P. S. (2018, March). "Study of AGC as two area thermal interconnected power system consisting WPG and SPG." In 2018 Emerging Trends in Electronic Devices and Computational Techniques (EDCT) (pp. 1-6). IEEE

[22] Singh, V. P., Mohanty, S. R., Kishor, N., & Ray, P. K. (2013). "Robust H-infinity load frequency control in hybrid distributed generation system." International journal of electrical power & energy systems, 46, 294-305.

[23] Hayerikhiyavi, M., & Dimitrovski, A. (2021, April). "A practical assessment of the power grid inertia constant using PMUs." In 2020 52nd North American Power Symposium (NAPS) (pp. 1-5). IEEE

[24] Audu, N. A., Alphaeus, O., & Adamu, T. (2018). "Effect of inertia constant on generator frequency and rotor angle." Eng. Appl. Sci, 3(1), 6.

[25] Tamrakar, U., Shrestha, D., Maharjan, M., Bhattarai, B. P., Hansen, T. M., & Tonkoski, R. (2017). "Virtual inertia: Current trends and future directions." Applied Sciences, 7(7), 654.

[26] Y. Chen, R. Hesse, D. Turschner, and H.-P. Beck, ''Improving the grid power quality using virtual synchronous machines,'' in Proc. Int. Conf. Power Eng. Energy Elect. Drives, May 2011.

[27] K. Ang, G. Chong, "PID Control System Analysis, Design, and Technology," IEEE Transactions on Control System Technology, Vol. 13, No. 4, July 2005

[28] E. Rakhshani, D. Remon, A. M. Cantarellas, J. M. Garcia, and P. Rodriguez, ''Virtual synchronous power strategy for multiple HVDC interconnections of multi-area AGC power systems,'' IEEE Trans. Power Syst., vol. 32, no. 3, pp. 1665–1677, May 2017.

[29] E. Rakhshani and P. Rodriguez, ‘‘Inertia emulation in AC/DC interconnected power systems using derivative technique considering frequency measurement effects,’’ IEEE Trans. Power Syst., vol. 32, no. 5, pp. 3338–3351, Sep. 2017.

[30] M. H. Finiand, M. E. H. Golshan, ‘‘Determining optimal virtual inertia and frequency control parameters to preserve the frequency stability in islanded microgrids with high penetration of renewables.’’ Electr. Power Syst. Res., vol. 154, no. 1, pp. 13–22, 2018.

[31] Millie Pant, RadhaThangaraj and Ajith Abraham, “Performance Tuning of Particle Swarm Optimization: An Investigation and Empirical Analysis”, Foundations on Computational Intelligence, Vol. 3: Global Optimization: Theoretical Foundations and Applications, Studies in Computational Intelligence Series, Springer Verlag, Germany, ISBN: 978-3-642-01084-2, pp. 101 – 128, 2009.

[32] R. Teodorescu, M. Liserre, and P. Rodriguez, Grid Converters for Photovoltaic and Wind Power Systems. Sussex, U.K.: Wiley, 2011.

[33] M. H. Finiand, M. E. H. Golshan, ‘‘Determining optimal virtual inertia and frequency control parameters to preserve the frequency stability in islanded microgrids with high penetration of renewables.’’ Electr. Power Syst. Res., vol. 154, no. 1, pp. 13–22, 2018.

[34] S. H. Liu, M. Mernik, ‘‘A parameter control method of evolutionary algorithms using exploration and exploitation measures with a practical application or fitting Sovova ’s mass transfer model,’’ Appl. Soft. Comput. vol.13, no.9, pp.3792–3805, Sep.2013.

[35] R. Teodorescu, M. Liserre, and P. Rodriguez, Grid Converters for Photovoltaic and Wind Power Systems. Sussex, U.K.: Wiley, 2011.

[36] R. Estes, The Behavior Guide to African Mammals: Including Hoofed Mammals, Carnivores, Primates, Illustrated. Oakland, CA, USA: Univ. California Press, 1992, pp. 235–248.

[37] J. Pastor, Y. Cohen, and N. T. Hobbs, ‘‘The roles of large herbivores in ecosystem nutrient cycles,’’ in Large Herbivore Ecology, Ecosystem Dynamics and Conservation, Conservation Biology. J. Pastor, K. Danell, P. Duncan R. Bergström, Eds. Cambridge, U.K.: Cambridge Univ. Press, 2006, pp. 289–325.

[38] T. Caro, A. Izzo, R. C. Reiner, H. Walker, and T. Stankowich, ‘‘The function of zebra stripes,’’ Nature Commun., vol. 5, no. 1, pp. 1–10, May 2014.

[39] A. M. Wilson et all, ‘‘Biomechanics of predator-prey arms race in lion, zebra, cheetah and impala” Nature. 2018 Feb 8;554(7691):183-188. doi: 10.1038/nature25479. Epub 2018 Jan 24.

[40] A. M. Wilson et all, ‘‘Biomechanics of predator-prey arms race in lion, zebra, cheetah and impala” Nature. 2018 Feb 8;554(7691):183-188. doi: 10.1038/nature25479. Epub 2018 Jan 24.

[41] Eva Trojovská, M. Dehghani and P. Trojovský, “Zebra Optimization Algorithm: A New Bio-Inspired Optimization Algorithm for Solving Optimization Algorithm.” January 2022 IEEE Access 10:1-1, DOI: 10.1109/ACCESS.2022.3172789.